Molecular Catalysis 507 (2021) 111549

Contents lists available at ScienceDirect

Molecular Catalysis

journal homepage: www.journals.elsevier.com/molecular-catalysis

Novel uric acid-based nano organocatalyst with phosphorous acid tags: Application for synthesis of new biologically-interest pyridines with indole moieties via a cooperative vinylogous anomeric based oxidation

Sima Kalhor [a], Mahmoud Zarei [a,*], Hassan Sepehrmansourie [a], Mohammad Ali Zolfigol [a,*], Hu Shi [b,*], Jinping Wang [c], Jalal Arjomandi [d], Masoumeh Hasani [e], Romana Schirhagl [f]

[a] Department of Organic Chemistry, Faculty of Chemistry, Bu-Ali Sina University, PO Box 6517838683, Hamedan, Iran
[b] School of Chemistry and Chemical Engineering, Institute of Molecular Science, Shanxi University, Taiyuan, 030006, China
[c] Institute of Surface Analysis and Chemical Biology, University of Jinan, Jinan, Shandong, 250022, China
[d] Department of Physical Chemistry, Faculty of Chemistry, Bu-Ali Sina University, 65178, Hamedan, Iran
[e] Department of Analytical Chemistry, Faculty of Chemistry, Bu-Ali Sina University, Hamedan, Iran
[f] University Medical Center Groningen, Groningen University, Antonius Deusinglaan 1, 9713 AV, Groningen, Netherlands

ARTICLE INFO

Keywords:
(2-Methyl-1*H*-indol-3-yl)-pyrazolo[3,4-*b*] pyridine
Phosphorous acid
theacrine tetrakis (phosphonic acid) (TTPA)
Uric acid
Vinyligous anomeric based oxidation

ABSTRACT

In this study, we have designed, synthesized and full characterized a novel biological based acidic nano organocatalyst via condensations reaction of uric acid and phosphorous acid. The obtained compound was named theacrine tetrakis(phosphonic acid) (TTPA) and prepared under refluxing ethanol. This new nano organocatalyst was applied as an efficient and recyclable catalyst for the preparation of novel pyridines with indole moieties via a cooperative vinylogous anomeric based oxidation with good to excellent yields.

1. Introduction

In recent years, the design and application of biological-basedcatalysts in organic synthesis and functional groups transformation have attracted intensive attention in the science and industry because of their unique properties, such as biodegradable ability, efficiency, reusability, reactivity, stability, selectivity, and easy separation of the catalyst [1–8]. The application of biological-based acidic organocatalysts in chemical processes has already been fully investigated [9]. The development of biological-based compounds with acidic groups (SO_3H and PO_3H_2) as solid acids has been the subject of enormous interest because of their interesting features such as nano-structures, thermal stability, and environmental friendliness [10–12]. Recent advances in organocatalytic cascade reactions toward the formation of quaternary stereocenters has been also comprehensively reviewed [13].

Uric acid (7,9-dihydro-1*H*-purine-2,6,8(3*H*)-trione), as a biological urea like structure, is known of having free-radical-scavenging property in human serum and blood and antioxidant activity. Different electrochemical, optical sensors and biosensors have been developed for sensitive and selective detection of uric acid in the field of disease diagnosis and treatment. Therefore, this compound has different applications in chemical and biochemical processes [14]. Among different properties of uric acid one can point to capability of increasing serum antioxidant capacity, adsorption of concomitant macromolecules particularly proteins, being a diagnostic marker of neurodegenerative diseases, and lowering blood glucose level [15].

Phosphorus as essential mineral for all living things, is naturally found in the body. In conjunction with calcium, phosphorus contributes to the formation of healthy bones and teeth [16]. Furthermore, it is an important nutrient for biochemical reactions in plants which are needed for plant's growth and puberty. It also plays an important role in photosynthesis, cell division, respiration, energy transfer and storage [17,18]. Recently, catalysts with phosphorous acid tags have been prepared and applied in organic synthesis [19].

Pyridine and its corresponding derivatives are unique heterocycles with worthwhile chemical and pharmaceutical importance, both in nature and synthesis plans. It has widely been used as key scaffold for design and preparation of novel drug candidate materials [20–25], supramolecular structures [26,27], polymers [28], and catalysts [29–31]. The essential vitamin B_6, nicotine, redox NADP-$NADPH_2$ coenzymes and

* Corresponding authors.
E-mail addresses: mahmoud8103@yahoo.com (M. Zarei), zolfi@basu.ac.ir (M.A. Zolfigol), hshi@sxu.edu.cn (H. Shi).

https://doi.org/10.1016/j.mcat.2021.111549
Received 14 January 2021; Received in revised form 21 March 2021; Accepted 24 March 2021
Available online 20 April 2021

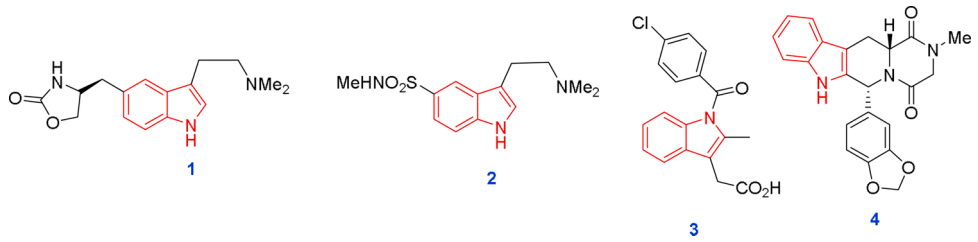

Fig. 1. The molecular structure of four drugs with indole moieties.

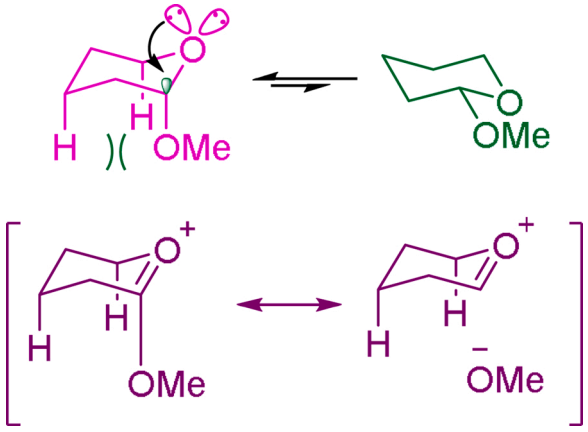

Fig. 2. Anomeric effect leads to the abnormal conformational preference.

many other natural products possess pyridine ring in their structures so it is quite rational that pyridine-containing compounds continue to receive great synthetic attention in organic chemistry [32–35]. On the other hand, indole derivatives, which are another important class of nitrogen containing heterocyclic compounds, also play notable role as targets in synthesis of a variety of drugs such as zolmitriptan (migraine: 1), sumatriptan (migraine:2), tadalafil (erectile dysfunction: 3) and indomethacin (anti-inflammatory :4). The structure of these indole-containing drugs is shown in Fig. 1 [36]. The application of indoles in multicomponent reactions [37] and the various synthetic strategies for synthesis of bis and tris indolyl methane's have been previously reviewed [38].

According to the alabugine's theory the stereoelectronic effects is a bridge between structure and reactivity and it has implications for many reactions, from classic to new [39,40]. The anomeric effect (AE) as a subset of stereoelectronic effects is the preference of certain substituents bonded to anomeric carbon for the axial position of the pyranose ring. The more stable axial configuration is explained by an orbital interaction. Anomeric effect as an oldest part of stereoelectronic effects is particularly important because it is a foundational concept that provides a basis for understanding reactivity of many organic, organometallic, and inorganic functional groups. It is a complicated effect because, as any other chemical phenomenon, it is related to molecular energies, conformations, and reactivity and depends on combination of factors, of which electrostatics and delocalization competition is of key importance [41–44]. In this phenomenon (i.e., AE), which is a kind of negative hyperconjugation, the electron density is delocalized from the lone-pair in a nonbonding orbital to the empty anti-bonding sigma orbital (n→σ*) (Fig. 2).

AE has been divided into different types including geminal (Endo, exo and reverse), vinylogous (Endo and exo) and so on (Fig. 3) [12]. This paper attempts to describe the role of vinylogous AE in the course of synthesis of target molecules for the first time [45]. Recently, we have introduced and developed the new term "anomeric based oxidation" (ABO) as a recent mechanistic viewpoint in the course of special reactions [46–52]. Cooperative geminal and vinylogous ABO has been well reviewed (Schemes 1 and 2) [53]. Due to this immensity, we wish to develop the application of the concept of ABO in new organic synthesis (Fig. 4).

In continuation of our investigation for developing biological based catalysts, we wish to introduce a novel uric acid-based organoctalyst with methylene phosphonic acid moieties as a derivative of theacrine namely theacrine tetrakis(phosphonic acid) (TTPA). Theacrine is a purine alkaloid which has been also known as 1,3,7,9-tetramethyluric acid. Theacrine is alike to caffeine molecule with additional methyl and carbonyl groups at 9 and 8-positions respectively [56]. This nano-organphosphorous acid was applied in the synthesis of novel 3-methyl-6-(2-methyl-1*H*-indol-3-yl)-1,4-diphenyl-1*H*-pyrazolo[3,4-*b*]

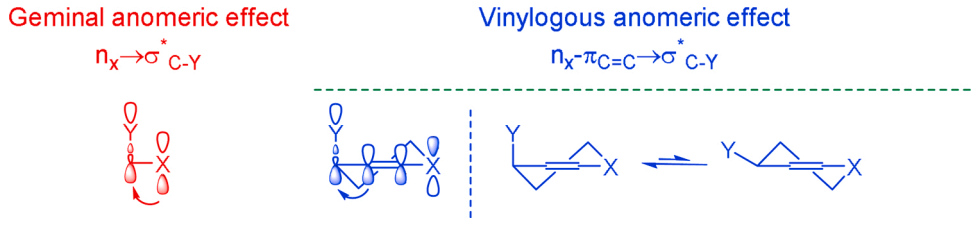

Fig. 3. Geminal anomeric effect versus the vinylogous anomeric effect.

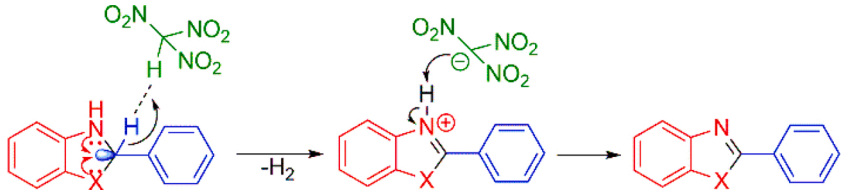

Scheme 1. A cooperative geminal anomeric based oxidation mechanism in the synthesis of 2-sbstituted benz-(imida, oxa and othia)-zoles [54].

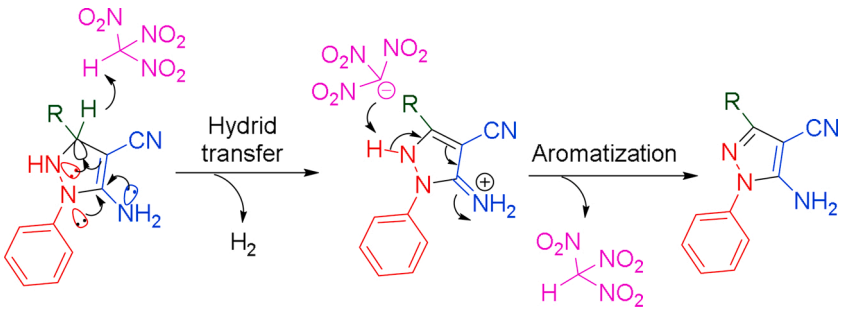

Scheme 2. A cooperative vinylogous anomeric based oxidation mechanism in the synthesis of 1,4-dihydropyrano-[2,3-*c*]-pyrazoles [55].

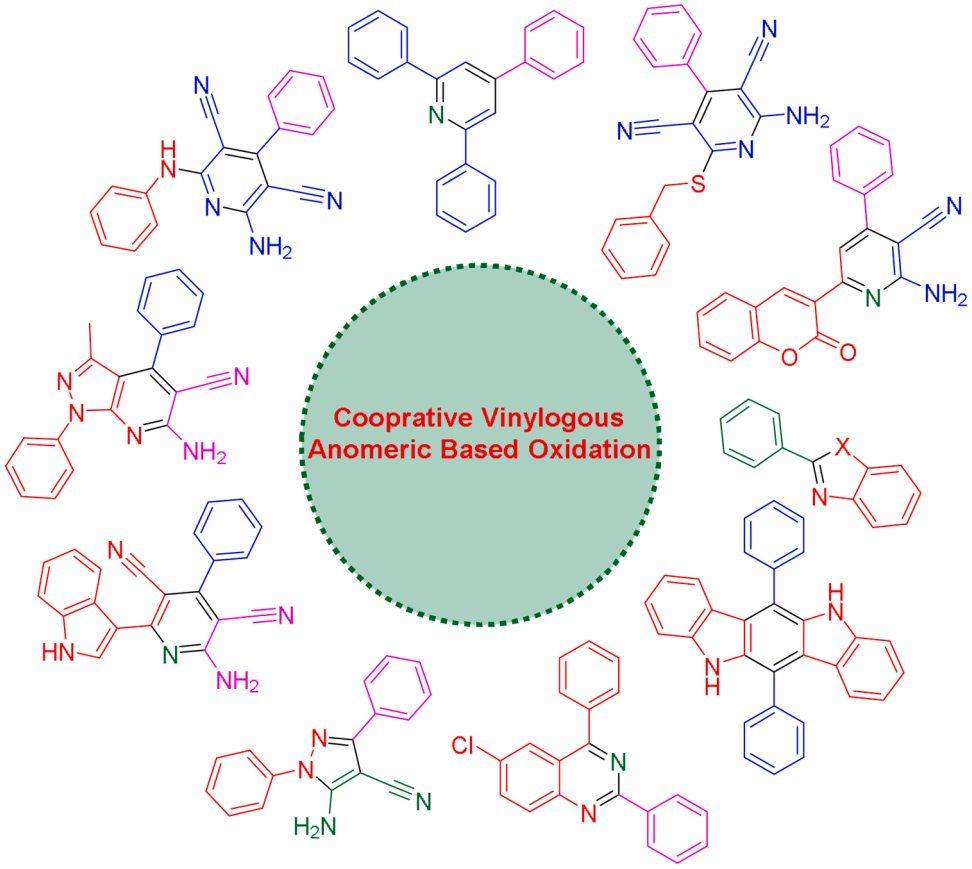

Fig. 4. Prepared aromatized molecules through a cooperative vinylogous anomeric based oxidation mechanism [5353b].

pyridine-5-carbonitrile and 6-(5-methoxy-2-methyl-1*H*-indol-3-yl)-3-methyl-1,4-diphenyl-1*H*-pyrazolo[3,4-*b*]pyridine-5-carbonitrile by reaction of various aromatic aldehydes, 3-methyl-1-phenyl-1*H*-pyrazol-5-amine and 3-(1*H*-indol-3-yl)-3-oxopropanenitrile derivatives under solvent-free at 110 °C (Scheme 3).

2. Experimental

2.1. Materials and methods

All chemicals were purchased from Merck Chemical Company. Silica gel SIL G/UV 254 plates were used for monitoring the progress of the reactions and purity tests. ^{1}H NMR and ^{13}C NMR spectra were recorded on a BRUKER Ultrashield FT-NMR spectrometer in DMSO-d_6 at frequencies of 600 or 400 MHz for proton and 151 or 101 MHz for carbon. Melting points were obtained on a Buchi B-545 apparatus using open capillary tubes. The infrared spectra of the synthesized compounds were recorded on a Perkin Elmer PE-1600-FTIR spectrometer. SEM was performed using a scanning electron microscope. The curves of thermogravimetric (TG), differential thermogravimetric (DTG) were recorded on Perkin Elmer Pyris 1 thermogravimetric analyzer at a temperature range of 25–600 °C and a heating rate of 10 °C/min. X-ray photoelectron spectroscopy (XPS) was carried out using Kratos Axis Ultra Spectrometer, equipped with an Al- Ka X-ray source (hn ¼ 1486.7 eV).

2.2. General procedure for the preparation of Theacrine tetrakis (phosphonic acid) (TTPA)

According to our previously reported procedures [48,49], in a 50 mL round-bottomed flask, a mixture of uric acid (1 mmol, 0.17 g), paraformaldehyde (4 mmol, 0.12 g), phosphorous acid (4 mmol, 0.32 g), *p*-TSA (10 mol%, 0.017 g) and 25 mL of ethanol were refluxed for 18 h. After this time, the resulting white precipitate was filtered off and dried under vacuum to give theacrine tetrakis(phosphonic acid) (Scheme 4).

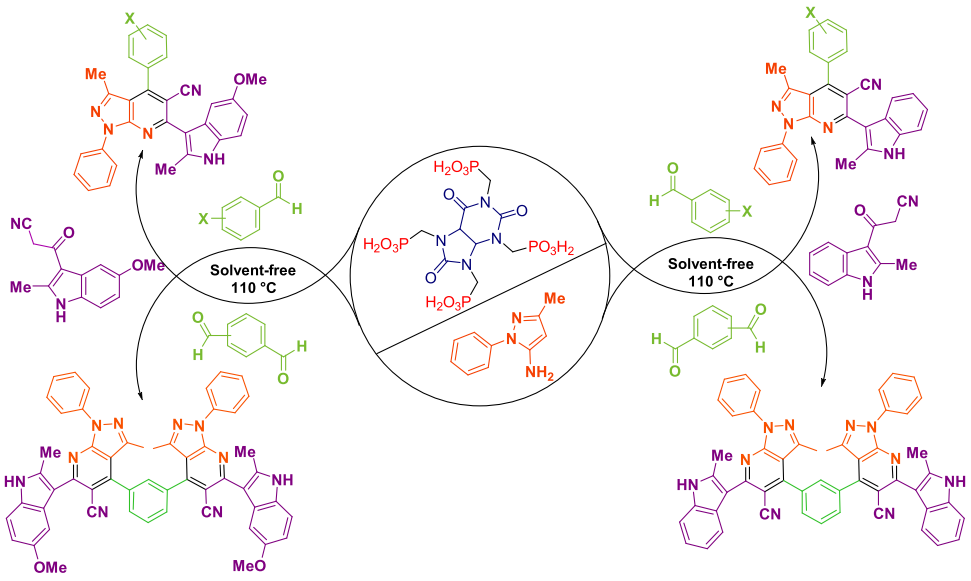

Scheme 3. Preparation of mono and bis-pyridines using theacrinete trakis(phosphonic acid) (TTPA) as a novel nano organocatalyst.

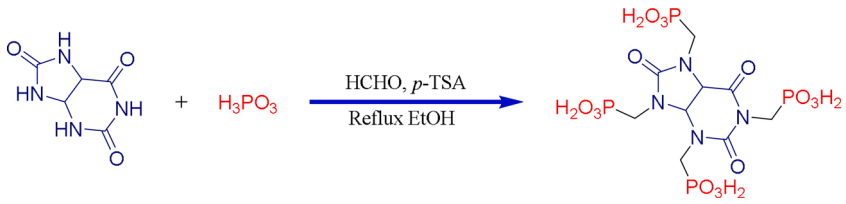

Scheme 4. Preparation of theacrine tetrakis(phosphonic acid) (TTPA).

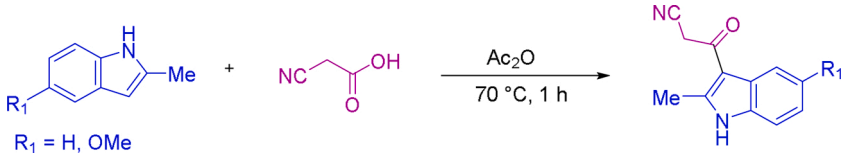

Scheme 5. Preparation of 3-(1*H*-indol-3-yl)-3-oxopropanenitrile derivatives.

2.3. General procedure for the synthesis of (2-methyl-1H-indol-3-yl)-pyrazolo[3,4-b]pyridine derivatives using TTPA as catalyst

Initially,3-(1*H*-indol-3-yl)-3-oxopropanenitrile derivatives were synthesized according to the previously reported literature (Scheme 5) [47,57]. Then, a mixture of 3-methyl-1-phenyl-1*H*-pyrazol-5-amine (1 mmol, 0.174 g), aryl aldehyde (1 mmol), 3-(2-methyl-1-*H*-indol-3-yl)-3-oxopropanenitrile derivatives (1 mmol) and theacrine tetrakis(phosphonic acid) (10 mol%, 0.0054 g) as the reaction catalyst were stirred under solvent-free condition at 110 °C in a 25 mL round-bottomed flask. After completion of the reaction [monitored by TLC (*n*-hexane: ethyl acetate 1:1)] the catalyst was separated by centrifugation (2000 rpm) after adding polyethylene glycol (PEG, 5 mL) for 5 min. Finally, the mixture was filtered off and washed with ethanol (3 × 10 mL) and the desired pure product was obtained (Scheme 3).

2.3.1. Spectral data

2.3.1.1. 3-Methyl-6-(2-methyl-1H-indol-3-yl)-1-phenyl-4-(p-tolyl)-1H-pyrazolo [3,4-b]pyridine-5-carbonitrile (1a). White solid; Mp: 255−257 °C; IR (KBr): υ (cm^{-1}) = 3294, 3064, 2926, 2854, 2224, 1583, 1551. ^{1}H NMR (600 MHz, DMSO-d_6) δ 11.67 (s, 1 H), 8.26 (d, *J* =7.9 Hz, 2 H), 7.67 (d, *J* =7.9 Hz, 1 H), 7.61 (d, *J* =7.8 Hz, 2 H), 7.55 (t, *J* =7.9 Hz, 2 H), 7.46 (d, *J* =7.8 Hz, 2 H), 7.42 (d, *J* =7.8 Hz, 1 H), 7.34 (t, *J* =7.4 Hz, 1 H), 7.15 (t, *J* =7.4 Hz, 1 H), 7.09 (t, *J* =7.8 Hz, 1 H), 2.59 (s, 3 H), 2.47 (s, 3 H), 2.12 (s, 3 H).^{13}C NMR (101 MHz, DMSO-d_6) δ 156.7, 152.2, 150.1, 143.8, 139.5, 138.4, 137.4, 135.0, 130.8, 129.1, 129.1, 129.0, 126.9, 126.2, 121.3, 120.6, 119.8, 118.8, 117.6, 112.3, 111.1, 111.0, 102.8, 20.9, 14.5, 13.2.

2.3.1.2. 4-(4-Bromophenyl)-3-methyl-6-(2-methyl-1H-indol-3-yl)-1-phenyl-1H-pyrazolo[3,4-b]pyridine-5-carbonitrile (2a). White solid; Mp: 298−300 °C; IR (KBr): υ (cm^{-1}) = 3213, 3184, 2926, 2211, 1666, 1571, 1546. ^{1}H NMR (600 MHz, DMSO-d_6) δ 11.70 (s, 1 H), 8.25 (d, *J* =7.9 Hz, 2 H), 7.95 (s, 1 H), 7.87 (d, *J* =8.3 Hz, 2 H), 7.71 (d, *J* =8.3 Hz, 2 H), 7.68 (d, *J* =8.0 Hz, 1 H), 7.55 (t, *J* =7.9 Hz, 2 H), 7.42 (d, *J* =8.0 Hz, 1 H), 7.35 (t, *J* =7.4 Hz, 1 H), 7.15 (t, *J* =7.5 Hz, 1 H), 7.09 (t, *J* =7.4 Hz, 1 H), 2.60 (s, 3 H), 2.12 (s, 3 H).^{13}C NMR (151 MHz, DMSO-d_6) δ 162.7, 157.2, 151.2, 150.6, 144.1, 138.8, 138.0, 135.5, 133.5, 132.01 131.8, 129.7, 127.3, 126.7, 124.1, 121.8, 121.1, 120.3, 119.3, 117.9, 112.7, 111.5, 103.2, 40.3, 40.2, 40.1, 39.9, 39.8, 39.6, 39.5, 36.2, 31.2, 15.0, 13.7.

2.3.1.3. 4-(4-Chlorophenyl)-3-methyl-6-(2-methyl-1H-indol-3-yl)-1-phenyl-1H-pyrazolo[3,4-b]pyridine-5-carbonitrile (3a). White solid; Mp: 272-*275* °C; IR (KBr): υ (cm^{-1}) = 3428, 3298, 3082, 2912, 2226, 1594,

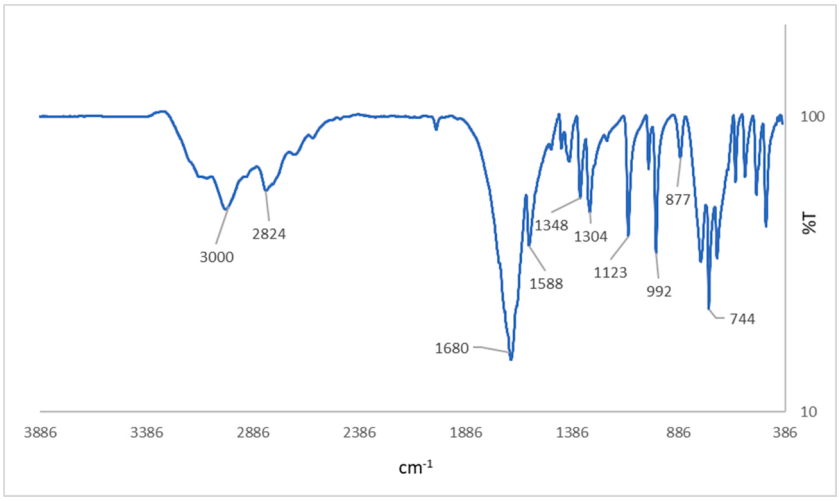

Fig. 5. FT-IR spectrum of TTPA.

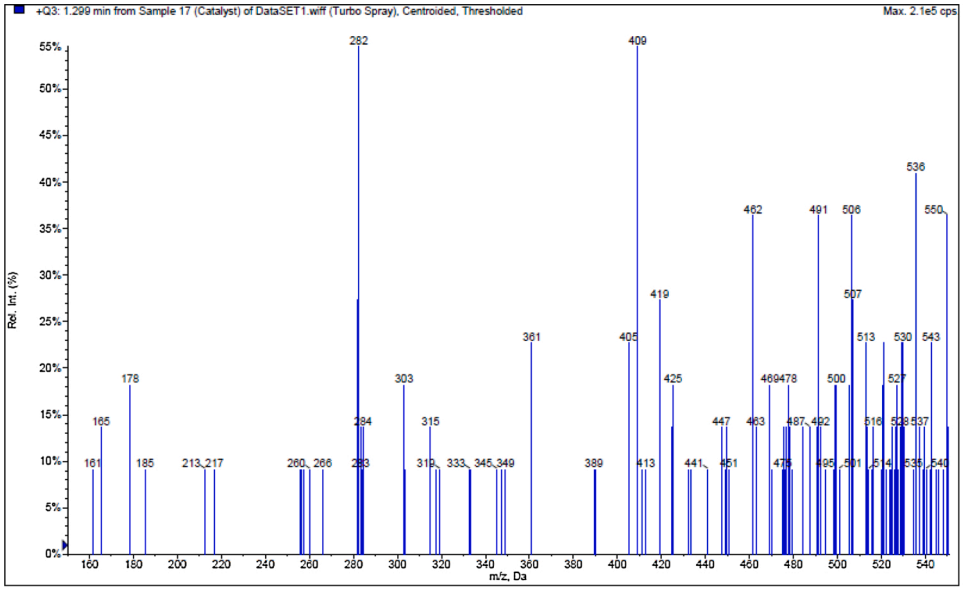

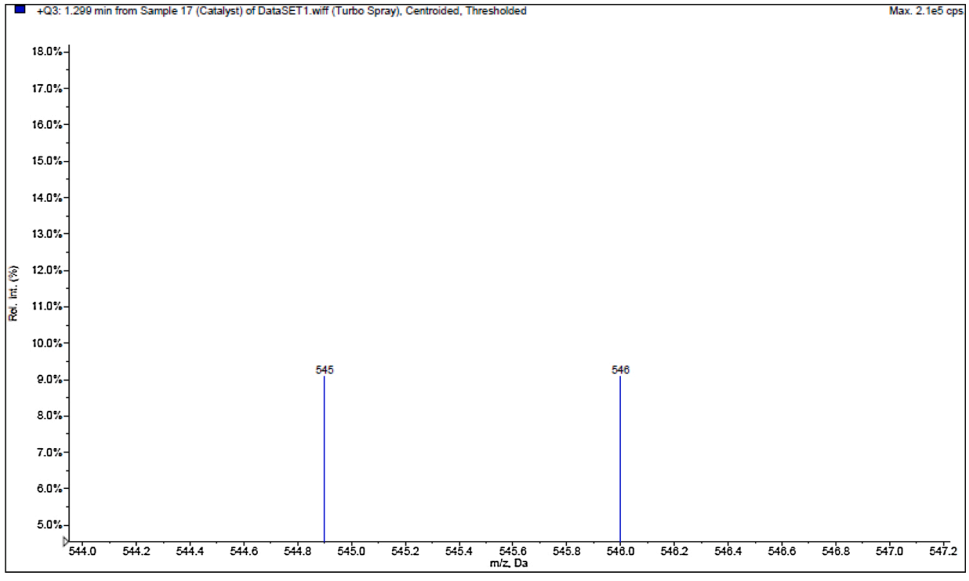

Fig. 6. Mass spectrum of TTPA.

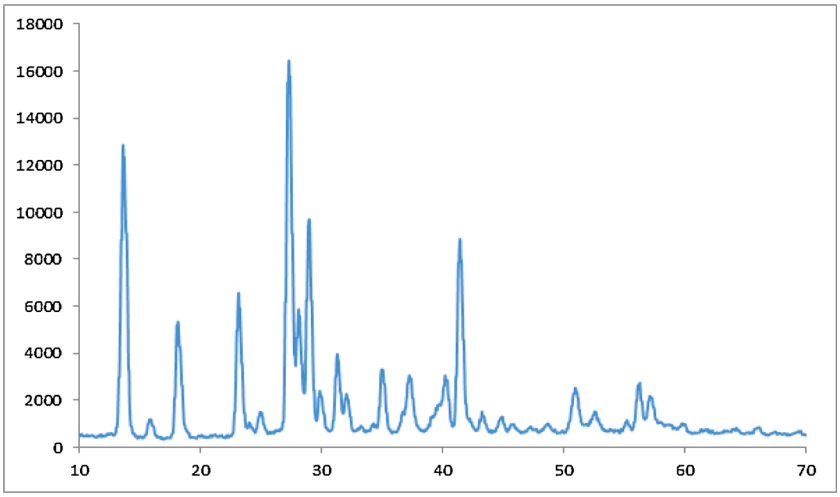

Fig. 7. XRD pattern of TTPA.

Table 1
XRD data of TTPA.

Entry	2θ	Peak width (degree)	Size [nm]	Inter planer distance[nm]
1	13.58	0.6	13.23	0.65
2	18.03	0.6	13.31	0.49
3	23.08	0.51	15.78	0.38
4	27.28	0.55	14.76	0.32
5	28.93	0.58	14.04	0.31
6	41.43	0.55	15.34	0.22

1573. ^{1}H NMR (600 MHz, DMSO-d_6) δ 11.70 (s, 1 H), 8.26 (d, J =8.1 Hz, 2 H), 7.79 (d, J =8.3 Hz, 2 H), 7.74 (d, J =8.3 Hz, 2 H), 7.68 (d, J =7.9 Hz, 1 H), 7.55 (t, J =7.8 Hz, 2 H), 7.42 (d, J =8.0 Hz, 1 H), 7.35 (t, J =7.4 Hz, 1 H), 7.15 (t, J =7.5 Hz, 1 H), 7.09 (t, J =7.5 Hz, 1 H), 2.60 (s, 3 H), 2.12 (s, 3 H).^{13}C NMR (151 MHz, DMSO-d_6) δ 157.2, 151.2, 150.6, 144.1, 138.8, 138.0, 135.5, 135.3, 133.1, 131.6, 129.7, 129.1, 127.3, 126.7, 121.8, 121.1, 120.3, 119.3, 117.9, 112.7, 111.5, 103.3, 40.3, 40.2, 40.1, 39.9, 39.8, 39.6, 39.5, 15.0, 13.7.

2.3.1.4. 3-Methyl-6-(2-methyl-1H-indol-3-yl)-1-phenyl-4-(o-tolyl)-1H-pyrazolo[3,4-b]pyridine-5-carbonitrile (4a). White solid; Mp: 255−258 °C; IR (KBr): υ (cm^{-1}) = 3412, 3061, 2923, 2215, 1601, 1567, 1507. ^{1}H NMR (600 MHz, DMSO-d_6) δ 11.69 (s, 1 H), 8.29 – 8.27 (m, 2 H), 7.66 (d, J =7.9 Hz, 1 H), 7.57 – 7.49 (m, 4 H), 7.48 (d, J =1.4 Hz, 1 H), 7.45 (dd, J = 7.4, 1.6 Hz, 1 H), 7.44 – 7.41 (m, 1 H), 7.37 – 7.31 (m, 1 H), 7.18 – 7.13 (m, 1 H), 7.12 – 7.07 (m, 1 H), 2.59 (s, 3 H), 2.20 (s, 3 H), 1.97 (s, 3 H).^{13}C NMR (151 MHz, DMSO-d_6) δ 157.2, 152.1, 150.6, 144.3, 138.9, 137.9, 135.6, 135.5, 134.0, 130.7, 130.2, 129.7, 129.1, 127.4, 126.6, 126.5, 121.9, 121.0, 120.4, 119.2, 117.6, 113.0, 111.5, 103.5, 40.5, 40.3, 40.2, 40.1, 39.9, 39.8, 39.6, 39.5, 19.7, 13.7, 13.7

2.3.1.5. 4-(4-Isopropylphenyl)-3-methyl-6-(2-methyl-1H-indol-3-yl)-1-phenyl-1H-pyrazolo[3,4-b]pyridine-5-carbonitrile (5a). White solid; Mp: 300−302 °C; IR (KBr): υ (cm^{-1}) = 3360, 3061, 2962, 2223, 1573, 1550. ^{1}H NMR (600 MHz, DMSO-d_6) δ 11.68 (s, 1 H), 8.26 (d, J =8.0 Hz, 2 H), 7.67 (d, J =7.9 Hz, 1 H), 7.64 (d, J =7.9 Hz, 2 H), 7.57 – 7.50 (m, 4 H), 7.42 (d, J =8.0 Hz, 1 H), 7.34 (t, J =7.4 Hz, 1 H), 7.15 (t, J =7.5 Hz, 1 H), 7.09 (t, J =7.4 Hz, 1 H), 3.05 (h, J =6.9 Hz, 1 H), 2.59 (s, 3 H), 1.31 (d, J =6.9 Hz, 6 H).^{13}C NMR (151 MHz, DMSO-d_6) δ 148.5, 148.3, 146.0, 146.0, 138.7, 137.6, 137.3, 135.5, 134.8, 130.9, 129.7, 129.6, 127.4, 127.3, 123.6, 123.5, 122.6, 122.6, 122.4, 121.69, 121.4, 121.1, 120.2, 119.0, 111.4, 106.1, 101.0, 84.1, 84.1, 56.4, 40.2, 40.0, 39.9, 39.8, 39.6, 19.0.

2.3.1.6. 4-(4-(Diethylamino) phenyl)-3-methyl-6-(2-methyl-1H-indol-3-yl)-1-phenyl-1H-pyrazolo [3,4-b]pyridine-5-carbonitrile (6a). White solid; Mp: 274−276 °C; IR (KBr): υ (cm^{-1}) = 3357, 3061, 2974, 2220, 1602, 1522, 1478. ^{1}H NMR (600 MHz, DMSO-d_6) δ 11.65 (s, 1 H), 8.26 (d, J =8.0 Hz, 2 H), 7.67 (d, J =7.9 Hz, 1 H), 7.53 (dd, J = 13.2, 8.1 Hz, 4 H), 7.41 (d, J =8.0 Hz, 1 H), 7.33 (t, J =7.4 Hz, 1 H), 7.14 (t, J =7.5 Hz, 1 H), 7.09 (t, J =7.4 Hz, 1 H), 6.87 (d, J =8.6 Hz, 2 H), 3.45 (q, J =6.9 Hz, 4 H), 2.59 (s, 3 H), 2.26 (s, 3 H), 1.17 (t, J =7.0 Hz, 6 H).^{13}C NMR (151 MHz, DMSO-d_6) δ 157.4, 153.3, 150.9, 149.0, 144.5, 139.0, 137.8, 135.5, 131.6, 129.6, 127.5, 126.5, 121.7, 121.1, 120.2, 119.6, 119.4, 118.9, 112.8, 111.8, 111.48, 110.8, 102.9, 44.1, 15.7, 13.8, 12.9.

2.3.1.7. 4-(4-Methoxyphenyl)-3-methyl-6-(2-methyl-1H-indol-3-yl)-1-phenyl-1H-pyrazolo[3,4-b]pyridine-5-carbonitrile (7a). White solid; Mp: 246−248 °C; IR (KBr): υ (cm^{-1}) = 3418, 3058, 2929, 2215, 1579, 1549. ^{1}H NMR (600 MHz, DMSO-d_6) δ 11.67 (s, 1 H), 8.26 (d, J =8.1 Hz, 2 H), 7.68 (d, J =8.1 Hz, 3 H), 7.55 (t, J =7.8 Hz, 2 H), 7.42 (d, J =8.0 Hz, 1 H), 7.34 (t, J =7.4 Hz, 1 H), 7.20 (d, J =8.4 Hz, 2 H), 7.14 (t, J =7.5 Hz, 1 H), 7.09 (t, J =7.5 Hz, 1 H), 3.89 (s, 3 H), 2.59 (s, 3 H), 2.16 (s, 3 H).^{13}C NMR (151 MHz, DMSO-d_6) δ 160.9, 157.3, 152.5, 150.6, 144.3, 138.9, 137.8, 135.5, 131.4, 129.6, 127.4, 126.6, 126.2, 121.8, 121.1, 120.3, 119.3, 118.2, 114.3, 113.0, 111.6, 111.4, 103.5, 55.8, 40.3, 40.2, 40.1, 39.9, 39.8, 39.6, 39.5, 15.2, 13.7.

2.3.1.8. 4-(4-fluorophenyl)-3-methyl-6-(2-methyl-1H-indol-3-yl)-1-phenyl-1H-pyrazolo [3,4-b]pyridine-5-carbonitrile (8a). White solid; Mp: 198−200 °C; IR (KBr): υ (cm^{-1}) = 3323, 3050, 2920, 2220, 1597. ^{1}H NMR (400 MHz, DMSO-d_6) δ 11.71 (s, 1 H), 8.26 (d, J =7.7 Hz, 2 H), 7.95 (s, 1 H), 7.81 (dd, J = 8.6, 5.4 Hz, 2 H), 7.69 (d, J =7.8 Hz, 1 H), 7.56 – 7.47 (m, 4 H), 7.43 (d, J =7.9 Hz, 1 H), 7.34 (t, J =7.4 Hz, 1 H), 7.15 (t, J =7.0 Hz, 1 H), 7.09 (t, J =7.0 Hz, 1 H), 2.61 (s, 3 H), 2.10 (s, 3 H).^{13}C NMR (101 MHz, DMSO-d_6) δ 164.2, 162.3, 161.7, 156.7, 151.0, 150.1, 143.7, 138.3, 137.5, 135.0, 131.7, 131.6, 130.1, 130.1, 129.1, 126.9, 126.2, 121.3, 120.6, 119.8, 118.8, 117.5, 115.6, 115.4, 112.4, 111.0, 111.0, 103.0, 39.8, 39.6, 39.4, 39.2, 39.0, 35.7, 30.7, 14.4, 13.2.

2.3.1.9. 4-(2-Bromo-4-methoxyphenyl)-3-methyl-6-(2-methyl-1H-indol-3-yl)-1-phenyl-1H-pyrazolo [3,4-b]pyridine-5-carbonitrile (9a). White solid; Mp: 172−175 °C; IR (KBr): υ (cm^{-1}) = 3388, 3326, 2926, 2840, 2222, 1600, 1555, 1458. ^{1}H NMR (600 MHz, DMSO-d_6) δ 11.72 (s, 1 H), 8.27 (d, J =7.7 Hz, 2 H), 7.68 – 7.64 (m, 2 H), 7.56 (t, J =8.0 Hz, 2 H), 7.52 (d, J =2.5 Hz, 1 H), 7.43 (d, J =8.0 Hz, 1 H), 7.35 (t, J =7.4 Hz, 1 H), 7.24 (dd, J = 8.5, 2.5 Hz, 1 H), 7.16 (t, J =7.2 Hz, 1 H), 7.10 (t, J =7.4 Hz, 1 H), 3.92 (s, 3 H), 2.59 (s, 3 H), 2.08 (s, 3 H).^{13}C NMR (151 MHz, DMSO-d_6) δ 161.3, 157.1, 150.9, 150.6, 144.1, 138.8, 138.0, 135.6, 131.9,

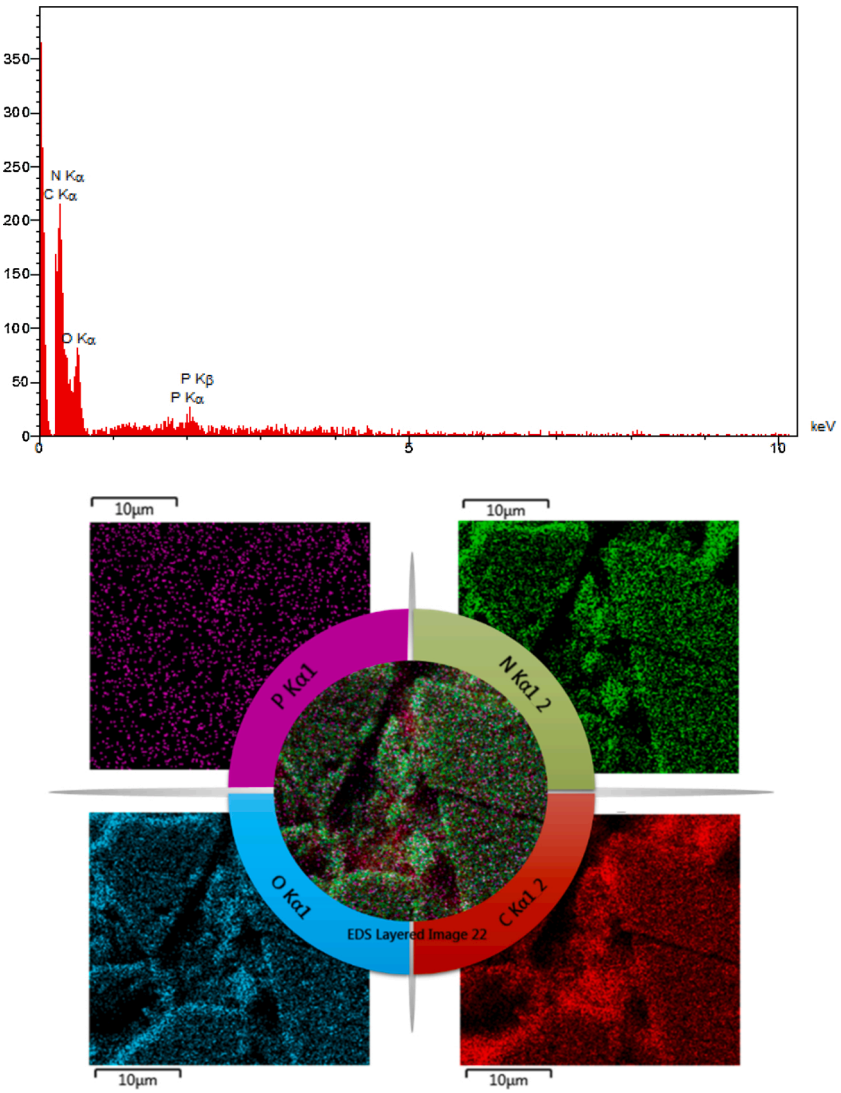

Fig. 8. (a) Energy dispersive X-ray spectroscopy (EDX) and (b) SEM-elemental mapping of TTPA.

129.7, 127.3, 127.2, 126.7, 122.6, 121.9, 121.1, 120.4, 119.2, 118.1, 117.4, 114.6, 113.2, 111.6, 111.4, 104.2, 56.3, 40.3, 40.2, 40.1, 39.9, 39.8, 39.6, 39.5, 13.9, 13.7.

2.3.1.10. 4-(4-fluorophenyl)-6-(5-methoxy-2-methyl-1H-indol-3-yl)-3-methyl-1-phenyl-1H-pyrazolo [3,4-b]pyridine-5-carbonitrile(1b). White solid; Mp: 280−282 °C; IR (KBr): υ (cm^{-1}) = 3332, 2967, 2221, 1604, 1560. ^{1}H NMR (600 MHz, DMSO-d_6) δ: 11.55 (s, 1 H), 8.30 (d, 2 H), 7.84 – 7.78 (m, 2 H), 7.57 – 7.49 (m, 4 H), 7.37 – 7.28 (m, 3 H), 6.79 (dd, *J* = 8.7, 2.5 Hz, 1 H), 3.72 (s, 3 H), 2.56 (s, 3 H), 2.11 (s, 3 H).^{13}C NMR (101 MHz, DMSO-d_6) δ 164.2, 161.7, 156.7, 154.1, 151.1, 150.1, 143.7, 138.4, 138.0, 131.6, 131.6, 130.2, 130.0, 129.1, 127.5, 126.2, 120.6, 117.5, 115.7, 115.4, 112.4, 111.6, 111.4, 111.1, 102.7, 100.9, 55.1, 40.0, 39.8, 39.6, 39.4, 39.2, 39.0, 38.8, 14.4, 13.6.

2.3.1.11. 6-(5-Methoxy-2-methyl-1H-indol-3-yl)-3-methyl-1-phenyl-4-(p-tolyl)-1H-pyrazolo [3,4-b]pyridine-5-carbonitrile(2b). White solid; Mp: 291−293 °C; IR (KBr): υ (cm^{-1}) = 3315, 3003, 2921, 2220, 1622, 1590, 1574. ^{1}H NMR (600 MHz, DMSO-d_6) δ 11.53 (s, 1 H), 8.30 (d, *J* =7.7 Hz, 2 H), 7.61 (d, *J* =8.0 Hz, 2 H), 7.55 (t, *J* =8.0 Hz, 2 H), 7.47 (d, *J* =7.9 Hz, 2 H), 7.35 (t, *J* =7.4 Hz, 1 H), 7.30 (d, *J* =8.7 Hz, 1 H), 7.27 (d, *J* =2.4 Hz, 1 H), 6.78 (dd, *J* = 8.7, 2.4 Hz, 1 H), 3.73 (s, 3 H), 2.55 (s, 3 H), 2.47 (s, 3 H), 2.12 (s, 3 H).^{13}C NMR (151 MHz, DMSO-d_6) δ 157.3, 154.6, 152.7, 150.7, 144.3, 140.0, 139.0, 138.4, 131.4, 130.5, 129.6, 129.6, 129.5, 128.0, 126.7, 121.1, 118.2, 112.8, 112.1, 111.9, 111.7, 103.1, 101.3, 55.6, 21.5, 15.0, 14.1.

2.3.1.12. 4-(5-cyano-6-(5-methoxy-2-methyl-1H-indol-3-yl)-3-methyl-1-phenyl-1H-pyrazolo [3,4-b]pyridin-4-yl)benzoic acid(3b). White solid; Mp: >300 °C; ^{1}H NMR (400 MHz, DMSO-d_6) δ 13.34 (s, 1 H), 11.56 (s, 1 H), 8.30 (d, *J* =7.7 Hz, 2 H), 8.20 (d, *J* =8.2 Hz, 2 H), 7.86 (d, *J* =8.2 Hz, 2 H), 7.57 (d, *J* =7.5 Hz, 2 H), 7.39 – 7.28 (m, 4 H), 6.79 (dd, *J* = 8.7, 2.2 Hz, 1 H), 3.73 (s, 3 H), 2.89 (s, 3 H), 2.08 (s, 3 H). ^{13}C NMR (101 MHz, DMSO-d_6) δ 166.8, 156.7, 154.1, 151.1, 150.1, 143.6, 138.4, 138.0, 132.0, 130.0, 129.5, 129.3, 129.1, 127.5, 126.3, 120.7, 117.4, 112.0, 111.6, 111.4, 102.3, 100.9, 55.1, 14.3, 13.6.

2.3.1.13. 6-(5-Methoxy-2-methyl-1H-indol-3-yl)-3-methyl-1-phenyl-4-(o-tolyl)-1H-pyrazolo [3,4-b]pyridine-5-carbonitrile(4b). White solid; Mp: 223−225 °C; IR (KBr): υ (cm^{-1}) = 3295, 2961, 2924, 2220, 1622, 1589, 1574. ^{1}H NMR (600 MHz, DMSO-d_6) δ 11.55 (s, 1 H), 8.32 (d, *J* =7.7 Hz, 2 H), 7.58 – 7.51 (m, 4 H), 7.49 – 7.44 (m, 2 H), 7.35 (t, *J* =7.4 Hz, 1 H), 7.31 (d, *J* =8.7 Hz, 1 H), 7.26 (s, 1 H), 6.79 (dd, *J* = 8.7, 2.4 Hz, 1 H), 3.73 (s, 3 H), 2.55 (s, 3 H), 2.22 (s, 3 H), 1.97 (s, 3 H).^{13}C NMR (151 MHz, DMSO-d_6) δ 157.2, 154.6, 152.2, 150.7, 144.3, 139.0, 138.4, 135.5, 134.1, 130.7, 130.5, 130.2, 129.6, 129.1, 128.0, 126.6, 126.5,

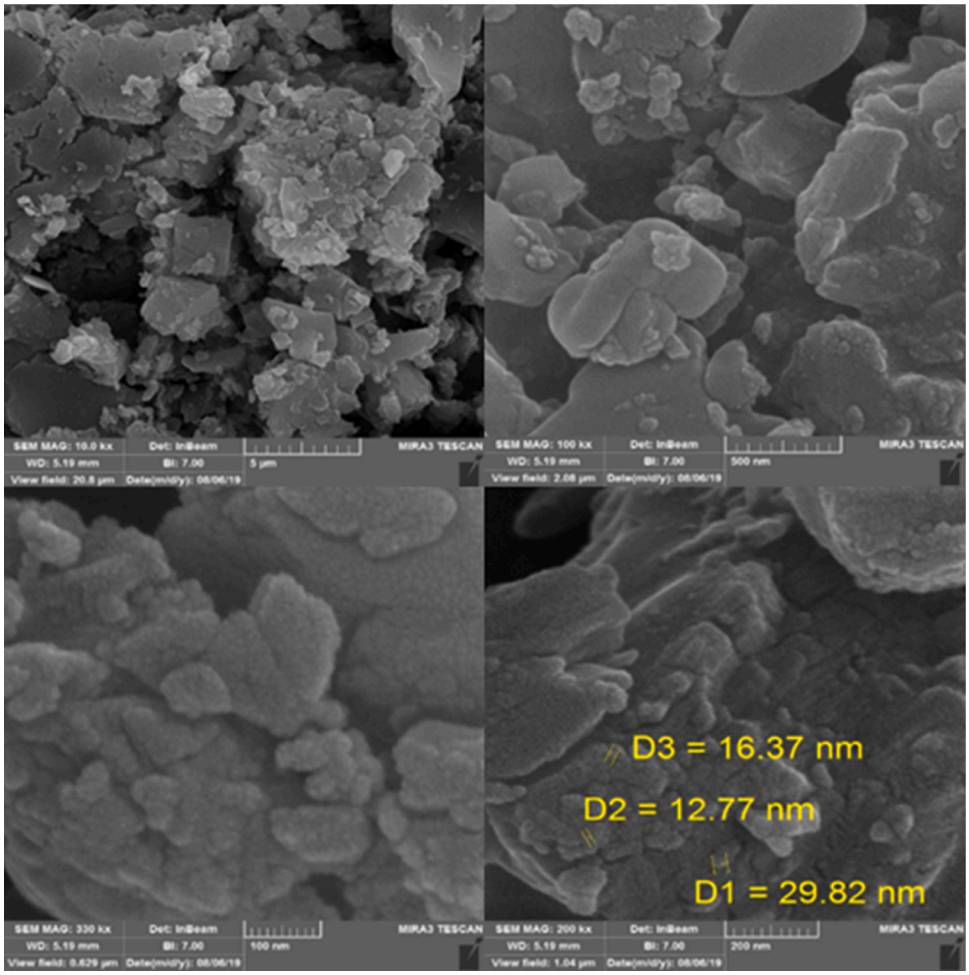

Fig. 9. Scanning electron microscopy (SEM) images TTPA.

121.0, 117.7, 113.0, 112.2, 111.9, 111.6, 103.2, 101.2, 55.5, 40.5, 40.3, 40.2, 40.1, 39.9, 39.8, 39.6, 39.5, 19.6, 14.1, 13.7.

2.3.1.14. 4-(4-(Diethylamino) phenyl)-6-(5-methoxy-2-methyl-1H-indol-3-yl)-3-methyl-1-phenyl-1H-pyrazolo [3,4-b]pyridine-5-carbonitrile(5b). White solid; Mp: 272−275 °C; IR (KBr): υ (cm^{-1}) = 3332, 2967, 2826, 2221, 1604, 1560, 1522. ^{1}H NMR (600 MHz, DMSO-d_6) δ 11.68 (s, 1 H), 8.26 (d, *J* =8.0 Hz, 2 H), 7.67 (d, *J* =7.9 Hz, 1 H), 7.64 (d, *J* =7.9 Hz, 2 H), 7.57 – 7.50 (m, 4 H), 7.42 (d, *J* =8.0 Hz, 1 H), 7.34 (t, *J* =7.4 Hz, 1 H), 7.15 (t, *J* =7.5 Hz, 1 H), 7.09 (t, *J* =7.4 Hz, 1 H), 3.05 (h, *J* =6.9 Hz, 1 H), 2.59 (s, 3 H), 1.31 (d, *J* =6.9 Hz, 6 H).^{13}C NMR (151 MHz, DMSO-d_6) δ 157.5, 154.5, 153.3, 151.0, 149.1, 144.4, 139.1, 138.2, 131.6, 130.5, 129.5, 128.1, 126.5, 121.1, 119.6, 119.0, 112.7, 112.1, 111.8, 111.8, 110.8, 102.7, 101.3, 55.6, 44.1, 15.7, 14.1, 12.9.

2.3.1.15. 4-(4-Bromophenyl)-6-(5-methoxy-2-methyl-1H-indol-3-yl)-3-methyl-1-phenyl-1H-pyrazolo [3,4-b]pyridine-5-carbonitrile(6b). White solid; Mp: 200−202 °C; IR (KBr): υ (cm^{-1}) = 3315, 3003, 2921, 2220, 1622, 1590, 1574. ^{1}H NMR (600 MHz, DMSO-d_6) δ 11.55 (s, 1 H), 8.30 – 8.29 (m, 2 H), 7.88 (d, *J* =8.4 Hz, 2 H), 7.71 (d, *J* =8.4 Hz, 2 H), 7.56 (m, 3 H), 7.36 (s, 1 H), 7.30 (d, *J* =8.7 Hz, 1 H), 7.28 (d, *J* =2.5 Hz, 1 H), 6.79 (dd, *J* = 8.7, 2.5 Hz, 1 H), 3.72 (s, 3 H), 2.56 (s, 3 H), 2.13 (s, 3 H).^{13}C NMR (151 MHz, DMSO-d_6) δ 157.2, 154.6, 151.3, 150.6, 144.1, 138.9, 138.5, 133.5, 132.0, 131.8, 130.5, 129.7, 128.0, 126.7, 124.1, 121.1, 118.0, 112.6, 112.1, 111.9, 111.6, 102.9, 101.4, 55.64, 15.0, 14.1.

2.3.1.16. 4-(4-chlorophenyl)-6-(5-methoxy-2-methyl-1H-indol-3-yl)-3-methyl-1-phenyl-1H-pyrazolo [3,4-b]pyridine-5-carbonitrile(7b). White solid; Mp: 272−275 °C; IR (KBr): υ (cm^{-1}) = 3332, 2998, 2929, 2219, 1622, 1592, 1573. ^{1}H NMR (400 MHz, DMSO-d_6) δ 11.56 (s, 1 H), 8.30 (d, *J* =7.7 Hz, 2 H), 7.80 – 7.72 (m, 4 H), 7.55 (t, *J* =8.0 Hz, 2 H), 7.38 – 7.27 (m, 3 H), 6.79 (dd, *J* = 8.7, 2.4 Hz, 1 H), 3.72 (s, 3 H), 2.56 (s, 3 H), 2.12 (s, 3 H).

2.3.1.17. 4-(2-Bromo-4-methoxyphenyl)-6-(5-methoxy-2-methyl-1H-indol-3-yl)-3-methyl-1-phenyl-1H-pyrazolo [3,4-b]pyridine-5-carbonitrile (8b). White solid; Mp: 230−234 °C; IR (KBr): υ (cm^{-1}) = 3291, 3009, 2929, 2223, 1599, 1575, 1505. ^{1}H NMR (600 MHz, DMSO-d_6) δ 11.59 (s, 1 H), 8.30 (d, *J* =7.9 Hz, 2 H), 7.65 (d, *J* =8.5 Hz, 1 H), 7.56 (t, *J* =7.9 Hz, 2 H), 7.53 (d, *J* =2.4 Hz, 1 H), 7.36 (t, *J* =7.4 Hz, 1 H), 7.31 (d, *J* =8.7 Hz, 1 H), 7.24 (dd, *J* = 8.4, 2.3 Hz, 2 H), 6.79 (dd, *J* = 8.7, 2.3 Hz, 1 H), 3.92 (s, 3 H), 3.73 (s, 3 H), 2.56 (s, 3 H), 2.08 (s, 3 H).^{13}C NMR (151 MHz, DMSO-d_6) δ 161.3, 157.1, 154.6, 151.0, 150.7, 144.1, 138.9, 138.5, 131.9, 130.5, 129.7, 127.8, 127.2, 126.7, 122.7, 121.0, 118.2, 117.5, 114.7, 113.1, 112.2, 112.0, 111.5, 103.9, 101.1, 56.34, 55.5, 14.0, 13.9.

2.3.1.18. 6-(5-Methoxy-2-methyl-1H-indol-3-yl)-4-(4-methoxyphenyl)-3-methyl-1-phenyl-1H-pyrazolo [3,4-b]pyridine-5-carbonitrile(9b). White solid; Mp: 200−202 °C; IR (KBr): υ (cm^{-1}) = 3316, 3001, 2929, 2221, 1608, 1576, 1555. ^{1}H NMR (600 MHz, DMSO-d_6) δ 11.52 (s, 1 H), 8.30 (d, *J* =7.7 Hz, 2 H), 7.67 (d, *J* =8.6 Hz, 2 H), 7.55 (t, *J* =7.9 Hz, 2 H), 7.35 (t, *J* =7.4 Hz, 1 H), 7.30 (d, *J* =8.7 Hz, 1 H), 7.27 (d, *J* =2.3 Hz, 1 H), 7.21 (d, *J* =8.7 Hz, 2 H), 6.78 (dd, *J* = 8.7, 2.4 Hz, 1 H), 3.90 (s, 3 H), 3.73 (s, 3 H), 2.56 (s, 3 H), 2.16 (s, 3 H).^{13}C NMR (151 MHz, DMSO-d_6) δ 160.9, 157.3, 154.6, 152.6, 150.7, 144.3, 139.0, 138.4, 131.4, 130.5,

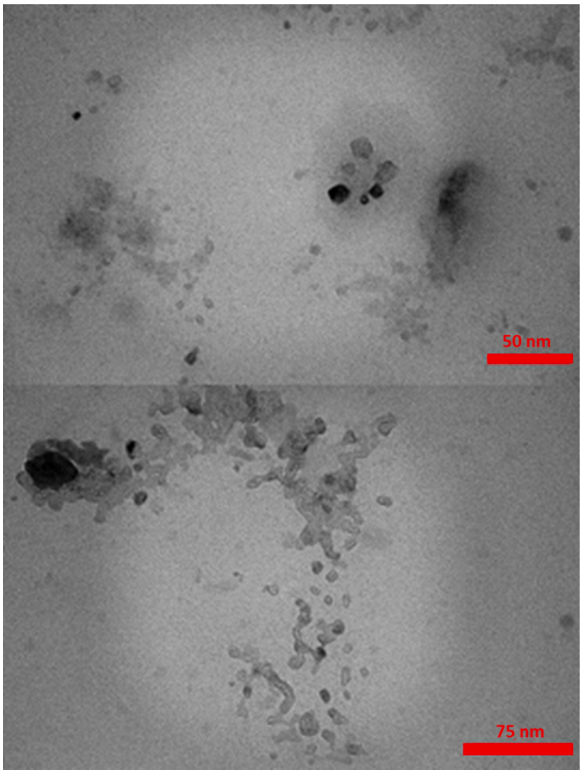

Fig. 10. Transmission electron microscopy (TEM) images TTPA.

129.6, 128.1, 126.6, 126.3, 121.1, 118.3, 114.3, 112.9, 112.1, 111.9, 111.7, 103.2, 101.3, 55.8, 55.6, 15.2, 14.1.

2.3.1.19. 6-(5-Methoxy-2-methyl-1H-indol-3-yl)-3-methyl-4-(2-nitrophenyl)-1-phenyl-1H-pyrazolo [3,4-b]pyridine-5-carbonitrile(10b). White solid; Mp: 241−244 °C; IR (KBr): υ (cm^{-1}) = 3295, 3071, 3003, 2221, 1622, 1593, 1577. ^{1}H NMR (600 MHz, DMSO-d_6) δ 11.60 (s, 1 H), 8.47 (d, *J* =8.3 Hz, 1 H), 8.30 (d, *J* =7.7 Hz, 2 H), 8.08 (dd, *J* = 7.5, 1.1 Hz, 1 H), 8.00 – 7.97 (m, 1 H), 7.93 (dd, *J* = 7.6, 1.2 Hz, 1 H), 7.57 (d, *J* =8.4 Hz, 2 H), 7.37 (d, *J* =7.4 Hz, 1 H), 7.31 (d, *J* =8.7 Hz, 1 H), 7.21 (s, 1 H), 6.79 (dd, *J* = 8.7, 2.4 Hz, 1 H), 3.73 (s, 3 H), 2.53 (s, 3 H), 2.01 (s, 3 H).^{13}C NMR (151 MHz, DMSO-d_6) δ 154.6, 150.7, 147.7, 143.8, 138.8, 138.5, 135.2, 132.3, 130.5, 129.7, 128.9, 127.8, 126.9, 125.8, 121.1, 112.3, 112.1, 111.4, 102.4, 55.5, 13.9, 13.9.

2.3.1.20. 4,4′-(1,3-Phenylene)bis(3-methyl-6-(2-methyl-1H-indol-3-yl)-1-phenyl-1H-pyrazolo[3,4-b]pyridine-5-carbonitrile)(1c). White solid; Mp: 282−284 °C; IR (KBr): υ (cm^{-1}) = 3323, 3058, 2920, 2220, 1597, 1505. ^{1}H NMR (600 MHz, DMSO-d_6) δ 11.70 (s, 2 H), 8.26 (d, *J* =7.9 Hz, 4 H), 7.96 (s, 1 H), 7.70 (d, *J* =8.0 Hz, 2 H), 7.58 – 7.52 (m, 6 H), 7.42 (d, *J* =7.9 Hz, 2 H), 7.35 (d, *J* =4.9 Hz, 2 H), 7.15 (d, *J* =4.7 Hz, 2 H), 7.08 (d, *J* =4.7 Hz, 2 H), 2.61 (s, 6 H), 2.17 (s, 6 H).

2.3.1.21. 4-(3-(5-Cyano-6-(4-methoxy-2-methyl-1H-indol-3-yl)-3-methyl-1-phenyl-1H-pyrazolo[3,4-b]pyridin-4-yl)phenyl)-6-(5-methoxy-2-methyl-1H-indol-3-yl)-3-methyl-1-phenyl-1H-pyrazolo[3,4-b]pyridine-5-carbonitrile(2c). White solid; Mp: 200−202 °C; IR (KBr): υ (cm^{-1}) = 3219, 3161, 2978, 2194, 1616, 1534, 1348. ^{1}H NMR (600 MHz, DMSO-d_6) δ 11.55 (s, 1 H), 8.30 (d, *J* =7.9 Hz, 2 H), 7.96 (d, *J* =3.2 Hz, 1 H), 7.58 – 7.53 (m, 3 H), 7.35 (d, *J* =7.2 Hz, 2 H), 7.32 (s, 1 H), 7.31 (d, *J* =3.2 Hz, 1 H), 6.79 (dd, *J* = 8.7, 2.1 Hz, 1 H), 3.72 (s, 3 H), 2.57 (s, 3 H), 2.17 (s, 3 H).^{13}C NMR (151 MHz, DMSO-d_6) δ 157.1, 151.8, 150.5, 144.4, 138.9, 138.0, 135.6, 135.0, 129.7, 127.4, 121.9, 121.2, 120.3, 113.1, 111.5, 103.6, 14.6, 13.7.

2.4. Cytotoxicity studies

Hela cells were cultured in dulbecco's modified eagle medium, supplemented with fetal bovine serum (10 %) and penicillin-streptomycin mixture (100 U/mL and 100 mg/mL) in humidified air containing 5% CO_2 at 37 °C. Hela cells were seeded on a 24-well plate, cultured for 12–24 hours, and then treated with 6a and 5b with different concentrations (0, 5, 10, 25, 50, 100 and 200 μM) for 72 h. Thereafter, the entire medium and cells from one well of the 24-well plate were

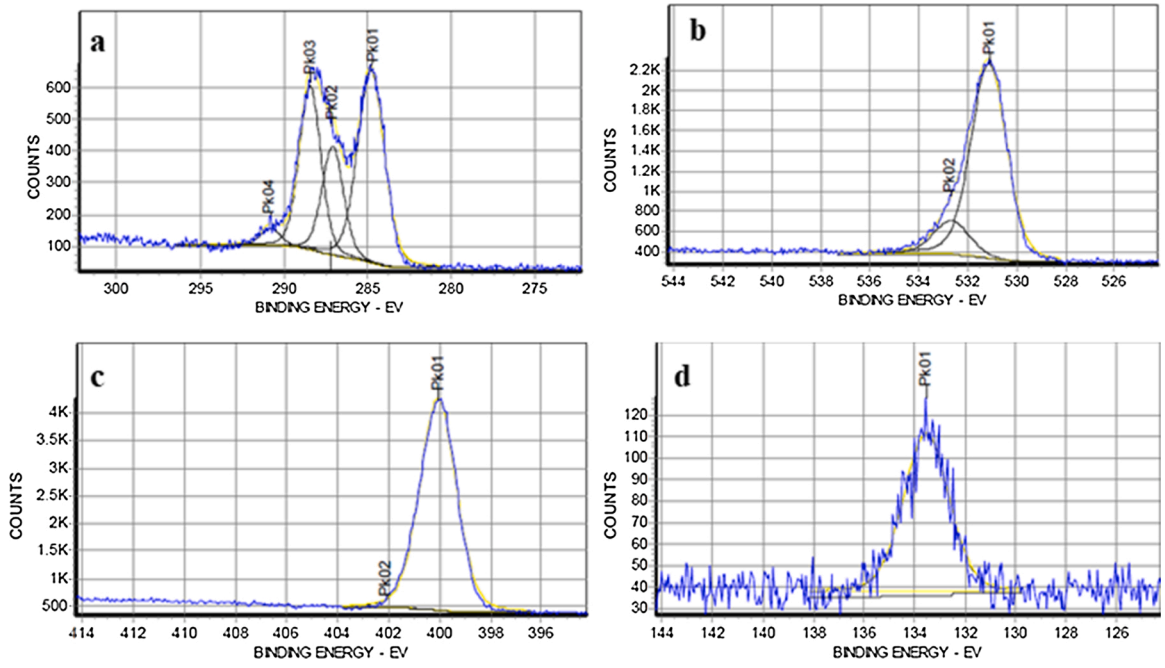

Fig. 11. X-ray photoelectron spectroscopy (XPS) of TTPA (a) C 1s, (b) O 1s, (c) N 1s and (d) P 2p spectra for the * film on metal.

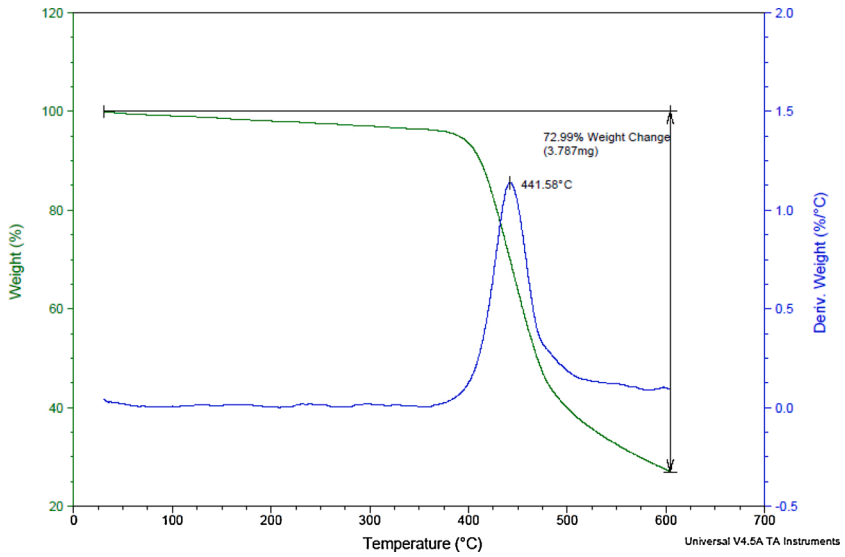

Fig. 12. Thermal gravimetric (TG) and derivative thermal gravimetric (DTG) of TTPA.

Table 2
Effect of different amounts of catalysts, temperature and solvent (5 mL) in the synthesis of (2-methyl-1*H*-indol-3-yl)-pyrazolo[3,4-*b*]pyridine derivatives.

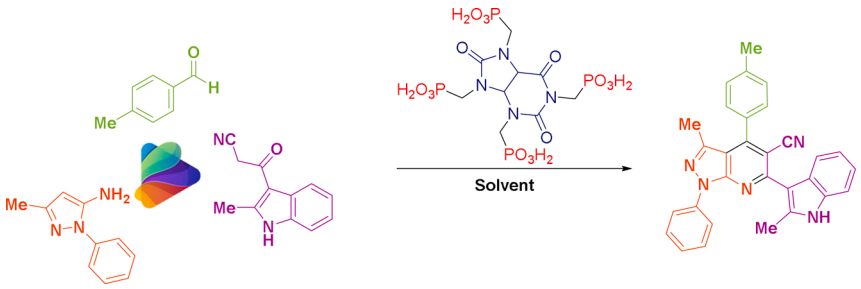

Entry	Solvent	Catalyst (mol%)	Temp. (°C)	Time (min)	Yield (%)
1	H_2O	10	Reflux	120	–
2	CH_3CN	10	Reflux	120	10
3	*n*-Hexane	10	Reflux	120	–
4	$CHCl_3$	10	Reflux	120	–
5	Toluene	10	Reflux	120	15
6	MeOH	10	Reflux	120	20
7	DMF	10	110	120	48
8	EtOH	10	Reflux	120	35
9	CH_2Cl_2	10	Reflux	120	–
10	EtOAc	10	Reflux	120	–
11	–	10	110	20	83
12	–	15	110	20	82
13	–	20	110	20	80
14	–	–	110	120	–
15	–	10	90	40	73
16	–	10	70	40	48
17	–	10	25	120	25

collected into a micro centrifuge tube. Cell viability was quantified by cell counting kit 8 (Beyotime Shanghai, China) assay in microplate reader (Model Spark, TECAN, Männedorf, Switzerland) according to the manufacturer's instruction.

3. Results and discussion

With the idea to show how stereoelectronic concepts can help chemists to build a conceptual bridge between structure and reactivity the synthesis of biological based uric acid (UA) with phosphorous acid functional groups was carried out. The structure of theacrine tetrakis (phosphonic acid) (TTPA) as nano-organocatalyst was thoroughly approved by FT-IR, Mass spectra, X-ray diffraction analysis (XRD), energy dispersive X-ray spectroscopy (EDX), SEM-elemental mapping, scanning electron microscope (SEM), transmission electron microcopy (TEM), XPS, thermal gravimetric (TG) and derivative thermal gravimetric (DTG). Then, the presented catalyst was used for the synthesis of novel (2-methyl-1*H*-indol-3-yl)-pyrazolo[3,4-*b*]pyridine derivatives as biological active candidates.

FT-IR spectrum of TTPA is shown in Fig. 5. The bands at 3000 and 2824 cm^{-1} are assigned to aromatic C–H stretching vibrations. Besides, the broad peak at 2800−3400 cm^{-1} is related to OH of PO_3H_2 functional groups. The absorption bands at 992 and 1055 cm^{-1} are related to P—O bond stretching and the band at 1123 cm^{-1} is related to P═O bond. Mass

Table 3
Synthesis of 3-methyl-6-(2-methyl-1*H*-indol-3-yl)-1,4-diphenyl-1*H*-pyrazolo[3,4-*b*]pyridine-5-carbonitrile derivatives by TTPA as a catalyst.

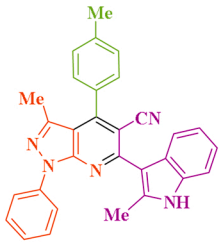

1a: Time (min): 15, Yield (%): 85
M.p (°C): 255-257

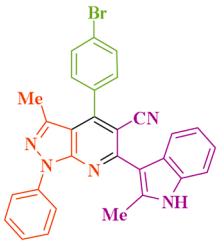

2a: Time (min): 18, Yield (%): 85
M.p (°C): 298-300

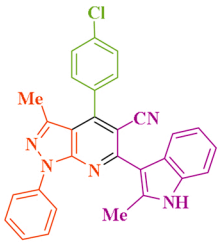

3a: Time (min): 12, Yield (%): 88
M.p (°C): 272-275

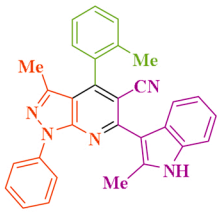

4a: Time (min): 25, Yield (%): 83
M.p (°C): 255-258

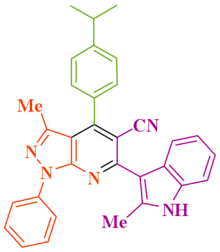

5a: Time (min): 15, Yield (%): 79
M.p (°C): 300-302

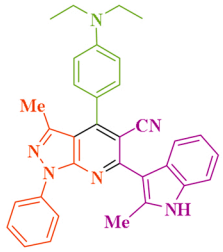

6a: Time (min): 25, Yield (%): 84
M.p (°C): 274-276

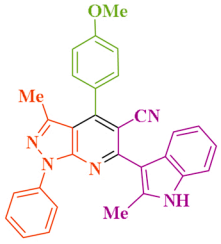

7a: Time (min): 15, Yield (%): 76
M.p (°C): 246-248

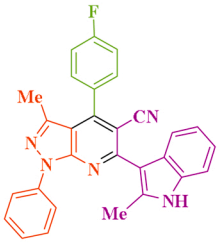

8a: Time (min): 20, Yield (%): 80
M.p (°C): 198-200

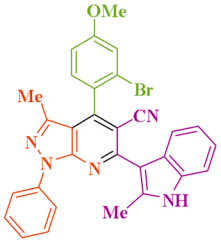

9a: Time (min): 30, Yield (%): 82
M.p (°C): 172-175

spectrum of TTPA is shown in Fig. 6. The mass spectrum of the catalyst gave the molecular ion peak at 545 *m/z* corresponding to its molecular formula.

The particle size of TTPA was examined by X-ray diffraction analysis (XRD) pattern in the 10–70 degrees (2θ) range. (Fig. 7). Debye-Scherrer formula $D = K\lambda/(\beta \cos\theta)$ and Bragg equation: $d_{hkl} = \lambda/(2 \sin.)$ were used for calculating crystal sizes in the nanometer range (13−16 nm) (Table 1). The results of XRD analysis revealed a regular structure in close agreement with the SEM images.

The elemental analysis and element distribution images of TTPA were obtained by methods of energy dispersive X-ray spectroscopy (EDX) and SEM-elemental mapping. The energy dispersive X-ray spectroscopy (EDX) was confirmed the existence of C, N, O and P atoms (Fig. 8a). Then, SEM-elemental mapping revealed uniformly distribution of elements throughout the sample C, N, O and P (Fig. 8b).

Morphology and particle size of TTPA were also studied by scanning electron microscopy (SEM) and transmission electron microscopy (TEM) images (Figs. 9 and 10). As shown, according to the obtained images from TTPA its particles size is in nano scale which are regularly arranged and not completely stacked.

The chemical composition of the TTPA was also confirmed by X-ray photoelectron spectroscopy (XPS). The XPS spectra showed the presence of carbon, oxygen, nitrogen, and phosphorus in the synthesized catalyst and peaks corresponding to C 1s (a); O 1s (b); N 1s (c) and P 2p (d) were detected (Fig. 11).

The broad C 1s peak (Fig. 11a) is divided into four peaks centered at 290.8, 288.4, 287.1 and 284.8 eV, separately. The peak at the higher binding energy (290.8, 288.4 and 287.1 eV) is due to the carbon making one double bond with oxygen and two bonds with nitrogen. The peaks with lower binding energy (284.8 eV) corresponds to the carbon making one double bond with oxygen, one bond with nitrogen and one bond with carbon, respectively [58]. Two broad O 1s peaks at 532.7 and 531.1 eV (Fig. 11b) indicate the different chemical states of oxygen. The peak at 531.1 eV is due to oxygen making a double bond with carbon and the other one at higher binding energy (532.7 eV) is attributed to the oxygen in phosphategroups [59]. The peaks at 400.1 and 402.1 eV (Fig. 11c) correspond to N 1s. Three C—N bonds are formed from overlap of nitrogen sp^2 hybride orbital with three carbon sp^2 orbitals (401.1–402.1 eV) [60]. The broad P 2p peak at 133.5 eV (Fig. 11d) is attributed to the phosphate group [61]. The XPS and FT-IR spectra were in good agreement for showing functional groups on the surface of the TTPA.

Thermal stability and structural of TTPA were also studied by thermal gravimetric (TG) and derivative thermal gravimetric (DTG) (Fig. 12). The first step of weight loss was found at 441 °C (includes about 60 % weight loss), which was linked to breaking the bond of N-C-PO_3H_2 in the structure of TTPA. This weight loss was related to removal of P_4O_{12} in the catalyst structure.

After the design, synthesis and identification of TTPA as an acidic organocatalyst, it was tested for the synthesis of new *N*-heterocycle derivatives such as (2-methyl-1*H*-indol-3-yl)-pyrazolo[3,4-*b*]pyridine derivatives. The synthesis of (2-methyl-1*H*-indol-3-yl)-pyrazolo[3,4-*b*] pyridine was selected as a model compound for optimization of reaction by applying 4-methyl benzaldehyde (1 mmol, 0.151 g), 3-methyl-1-phenyl-1*H*-pyrazol-5-amine (1 mmol, 0.174 g) and 3-(1*H*-indol-3-yl)-3-oxopropanenitrile (1 mmol, 0.198 g). The optimized reaction conditions are listed in Table 2. As shown, the best reaction conditions for the

Table 4
Synthesis of 6-(5-methoxy-2-methyl-1*H*-indol-3-yl)-3-methyl-1,4-diphenyl-1*H*-pyrazolo[3,4-*b*]pyridine-5-carbonitrile derivatives by TTPA as a catalyst.

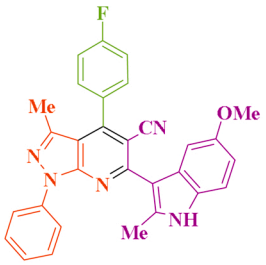

1b: Time (min): 20, Yield (%): 80
M.p (°C): 280-282

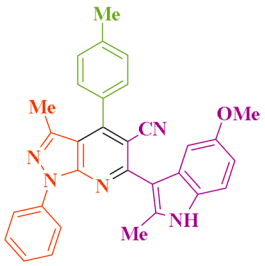

2b: Time (min): 20, Yield (%): 88
M.p (°C): 291-293

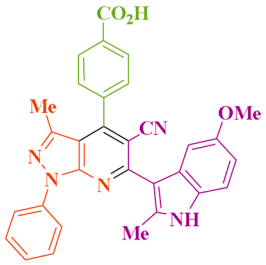

3b: Time (min): 20, Yield (%): 80
M.p (°C): >300

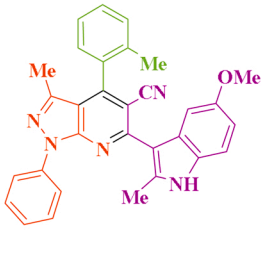

4b: Time (min): 25, Yield (%): 77
M.p (°C): 223-225

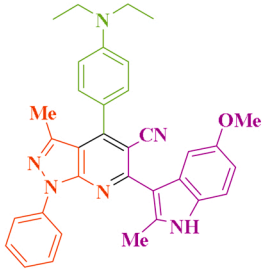

5b: Time (min): 25, Yield (%): 84
M.p (°C): 272-275

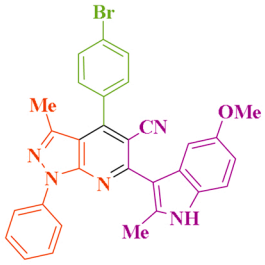

6b: Time (min): 20, Yield (%): 80
M.p (°C): 200-202

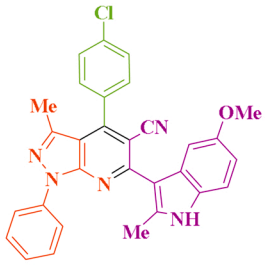

7b: Time (min): 15, Yield (%): 85
M.p (°C): 272-275

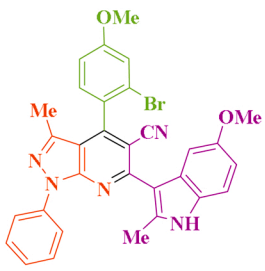

8b: Time (min): 22, Yield (%): 82
M.p (°C): 230-234

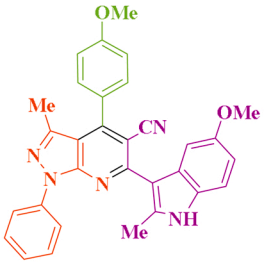

9b: Time (min): 20, Yield (%): 80
M.p (°C): 200-202

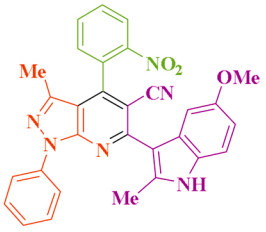

10b: Time (min): 28, Yield (%): 82
M.p (°C): 241-244

synthesis of (2-methyl-1*H*-indol-3-yl)-pyrazolo[3,4-*b*]pyridine was achieved in the presence of 10 mol% TTPA under solvent free condition at 110 °C (**entry 11,** Table 2). As seen from Table 2, the other experimental conditions used for the model reaction (i.e. different amounts of catalyst and various temperatures) resulted in no better improvement in reaction yield and time (**entries 12–17,** Table 2). The model reaction was also studied in the several solvents such as H_2O, CH_3CN, *n*-Hexane, $CHCl_3$, Toluene, MeOH, DMF, EtOH, CH_2Cl_2, EtOAc (10 mL) (**entries 1–10,** Table 2). Considering the obtained reaction yield and time, we chose the solvent-free condition in the presence of 10 mol% of the acrinetetrakis(phosphonic acid) as optimal experimental condition.

In the next step, TTPA was used as a nano heterogeneous organocatalyst, in the reaction of 3-methyl-1-phenyl-1*H*-pyrazol-5-amine (1 mmol, 0.174 g), aryl aldehyde (1 mmol) and 3-(2-methyl-1*H*-indol-3-yl)-3-oxopropanenitrile derivatives (1 mmol). As exposed in Table 3, the results show that this method is suitable for the synthesis of novel (2-methyl-1*H*-indol-3-yl)-pyrazolo[3,4-*b*]pyridine derivatives such as 3-methyl-6-(2-methyl-1*H*-indol-3-yl)-1,4-diphenyl-1*H*-pyrazolo[3,4-*b*] pyridine-5-carbonitrile and 6-(5-methoxy-2-methyl-1*H*-indol-3-yl)-3-methyl-1,4-diphenyl-1*H*-pyrazolo[3,4-*b*]pyridine-5-carbonitrile in high to excellent yields (82–95 %) in relatively short reaction time (4−20 min). As shown in Tables 3–5, all aldehydes including benzaldehyde as well as other aromatic aldehydes possessing electron-releasing substituents, electron withdrawing substituents, basic groups or halogens afforded the desired novel (2-methyl-1*H*-indol-3-yl)-pyrazolo[3,4-*b*] pyridine derivatives with good to excellent yields. Also, bis aromatic aldehydes (terphetaldehyde and iso-terphetaldehyde) produced their corresponding bis (2-methyl-1*H*-indol-3-yl)-pyrazolo[3,4-*b*]pyridines

Table 5
Synthesis of bis (2-methyl-1*H*-indol-3-yl)-pyrazolo[3,4-*b*]pyridine derivatives by TTPA as a catalyst.

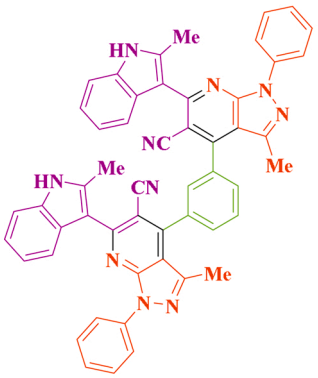

1c: Time (min): 30, Yield (%): 75
M.p (°C): 282-284

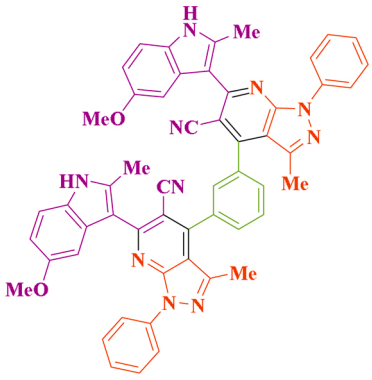

2c: Time (min): 20, Yield (%): 80
M.p (°C): 200-202

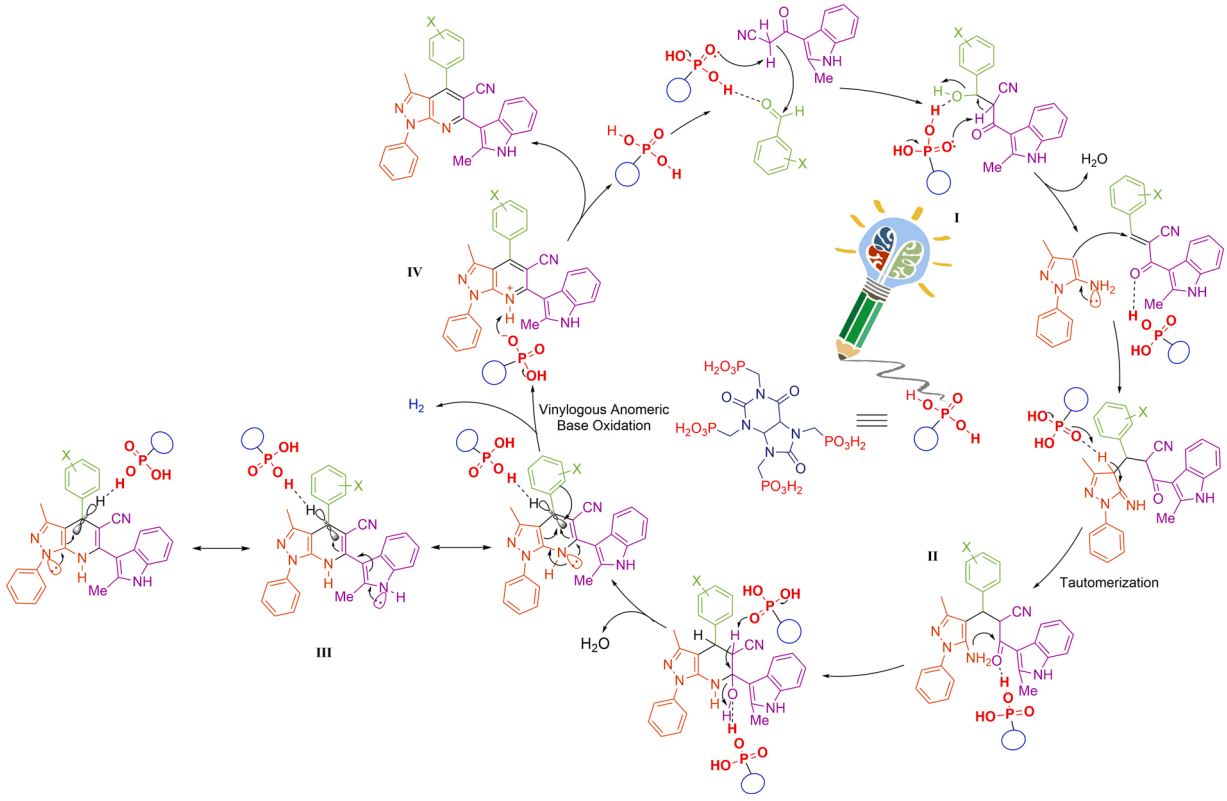

Scheme 6. Proposed mechanism for the synthesis (2-methyl-1*H*-indol-3-yl)-pyrazolo[3,4-*b*]pyridine derivatives using TTPA.

(Table 5).

In the proposed mechanism, aldehyde is activated with acidic functional groups of TTPA and intermediate (I) is prepared by reaction of 3-(1*H*-indol-3-yl)-3-oxopropanenitrile with the loss of one molecule of H_2O. In the second step, 3-methyl-1-phenyl-1*H*-pyrazol-5-amine reacts with intermediate (I) to give intermediate (II) after tautomerization. Then, intermediate (II) gives intermediate (III) after intramolecular cyclization and loss of one molecule of H_2O. We have recently introduced "cooperative vinylogous anomeric-based oxidations" based on the use of the vinylogous anomeric effect [53b] for the removal of hydride, a step needed to complete the final oxidation/aromatization in the synthesis of described pyridines. To approve the above-mentioned idea, reaction was achieved under both nitrogen and argon atmosphere and in the absence of any molecular oxygen. It was found that, the reaction proceeded under inert atmospheres (nitrogen and argon). These evidences attributed to the conversion of intermediate (III) to (IV by unusual hydride transfer and release of molecular hydrogen (H_2) by using TTPA. The C—H bond is weakened via a cooperative vinylogous anomeric supporting of the nitrogen lone pairs into the vacant anti-bonding of C–H (σ^*_{C-H} orbital) which can further react with a proton to provide molecular hydrogen (Scheme 6). The results obtained for the model reaction under argon and nitrogen atmospheres verified our suggestion for the final step.

The efficiency of TTPA for the synthesis of (2-methyl-1*H*-indol-3-yl)-

Table 6
Evaluation of various catalysts for the synthesis of (2-methyl-1*H*-indol-3-yl)-pyrazolo[3,4-*b*]pyridine in comparison with TTPA.

Entry	Catalyst	(mol %)	Time (min)	Yield (%)
1	CF_3SO_3H	10	30	25
2	$NaHSO_4$	10	45	–
3	*p*-TSA	10	30	25
4	$Al(HSO_4)_3$	10	60	–
5	TTPA	10	15	85[a]
6	$FeCl_3$	10	60	15
7	[Py-SO_3H]Cl [62]	10	30	65
8	[PVI-SO_3H]Cl [63]	10 mg	30	72
9	Et_3N	20	60	20
10	UA	10	60	trace
11	$Mg(NO_3)_2.6H_2O$	10	60	–
12	TrBr [64]	10	60	trace
13	[Fe_3O_4@SiO_2@$(CH_2)_3$-DABCO-SO_3H]Cl_2 [65]	10 mg	45	40
14	SSA [66]	10 mg	30	36
15	APVPB [67]	10 mg	30	53
16	H_3PO_2	10	60	45

[a] This work.

pyrazolo[3,4-*b*]pyridine was compared with many other catalysts in the reaction of 4-methyl benzaldehyde (1 mmol, 0.151 g), 3-methyl-1-phenyl-1*H*-pyrazol-5-amine (1 mmol, 0.174 g) and 3-(1*H*-indol-3-yl)-3-oxopropanenitrile (1 mmol, 0.198 g) under the above mentioned optimized reaction conditions. Various organic and inorganic acidic catalysts were also tested (Table 6). As Table 6 indicates, TTPA is the best choice for the synthesis of (2-methyl-1*H*-indol-3-yl)-pyrazolo[3,4-*b*]pyridine derivatives; regarding the shorter reaction times, higher yields and the amount of applied catalyst.

The reusability of the TTPA as catalyst for the preparation of (2-methyl-1*H*-indol-3-yl)-pyrazolo[3,4-*b*]pyridine derivatives was examined in the model reaction by using 4-methyl benzaldehyde (1 mmol, 0.151 g), 3-methyl-1-phenyl-1*H*-pyrazol-5-amine (1 mmol, 0.174 g) and 3-(1*H*-indol-3-yl)-3-oxopropanenitrile (1 mmol, 0.198 g). The results showed that the TTPA catalyst has the potential to be reused up to 5 times without significant decrease in its catalytic activity (Fig. 13). The recovered TTPA after the fifth run was also characterized by FT-IR and energy dispersive X-ray spectroscopy (EDX). These spectra were the same as those of the fresh catalyst (Figs. 14 and 15).

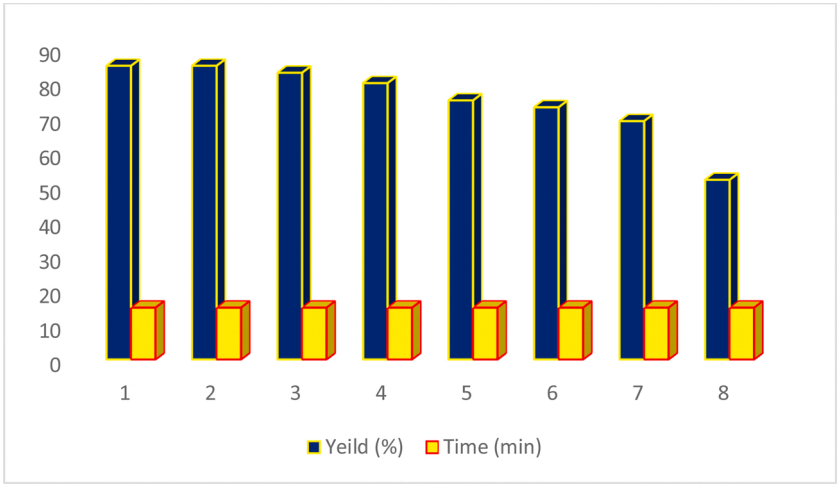

Fig. 13. Recyclability of TTPA at the synthesis (2-methyl-1*H*-indol-3-yl)-pyrazolo[3,4-*b*]pyridine derivatives.

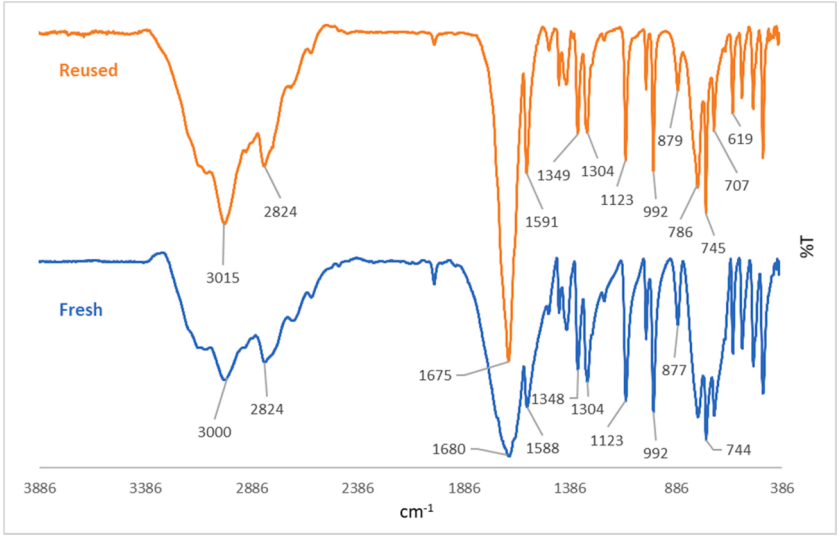

Fig. 14. FT-IR spectrum of fresh and recovered catalyst (TTPA).

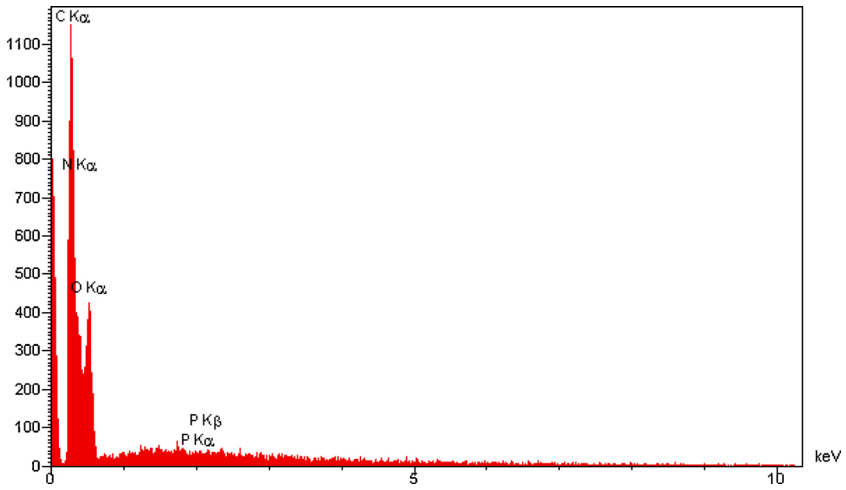

Fig. 15. Energy dispersive X-ray spectroscopy (EDX) of recyclability of TTPA.

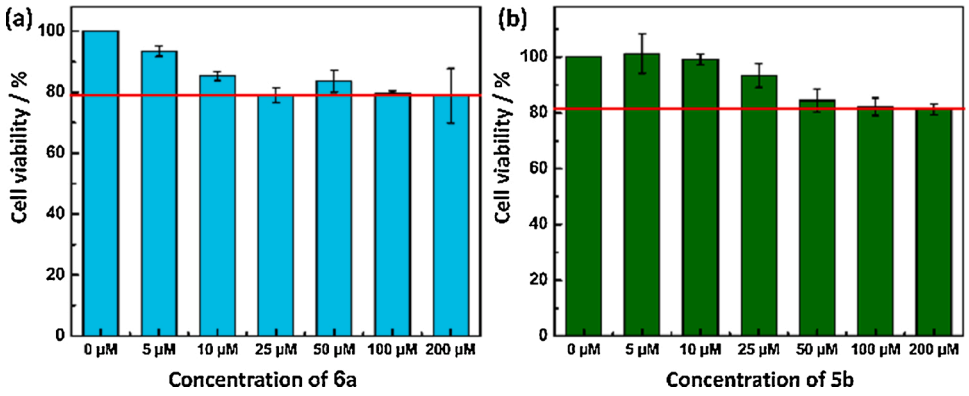

Fig. 16. Viability of Hela cells after being exposed to 6a(a) and 5b(b).

3.1. Cytotoxicity studies

Hela cells were incubated with 6a and 5b under the experimental condition mentioned in Section 2.4 to investigate the cytotoxicity and potential bio-applications of the compounds. As shown in Fig. 16a, after exposing Hela cells to 6a with the concentrations of 5, 10, 25, 50, 100 and 200 μM for 72 h, the viability of Hela cells was about 78.78 % for all concentrations, implying a low cytotoxicity of 6a. Similarly, the viability of Hela cells is greater than 81.3 % after being treated with 5b (5, 10, 25, 50, 100 and 200 μM) for 72 h (in Fig. 16b), indicating the biocompatibility of 5b is even higher than that of 6a. Consequently, it can be deemed that both biocompatible 6a and 5b can be further applied in biological assays.

4. Conclusions

In conclusion, we have designed and introduced theacrine tetrakis (phosphonic acid) (TTPA) as a novel biological nano-organocatalyst. The new catalyst was identified by various spectroscopic techniques. TTPA was used for the synthesis of new (3'-indolyl)pyrazolo[3,4-*b*] pyridine derivatives as biological active candidates according to the cooperative vinylogous anomeric based oxidation mechanism. Short reaction time, clean profile of reaction, recyclability of catalyst are advantages of the presented work.

Declaration of Competing Interest

The authors report no declarations of interest.

Acknowledgements

We thank the Bu-Ali Sina University and Iran National Science Foundation (INSF) (Grant Number: 98020070) for financial support.

Appendix A. Supplementary data

Supplementary material related to this article can be found, in the online version, at doi:https://doi.org/10.1016/j.mcat.2021.111549.

References

[1] Z. Chen, Q. Zhu, W. Su, Tetrahedron Lett. 52 (2011) 2601–2604, https://doi.org/10.1016/j.tetlet.2011.03.059.
[2] I.N. Martyanov, A. Sayari, Appl. Catal. A Gen. 339 (2008) 45–52, https://doi.org/10.1016/j.apcata.2008.01.007.
[3] Z. Li, Q. Yang, X. Qi, Y. Xu, D. Zhang, Y. Wang, X. Zhao, Chem. Commun. 51 (2015) 1930–1932, https://doi.org/10.1039/C4CC08273G.
[4] Y. Wang, J. Zhou, K. Liu, L. Dai, J. Mol. Catal. A Chem. 366 (2013) 195–201, https://doi.org/10.1016/j.molcata.2012.09.023.
[5] Y.M. Sani, W.M.A.W. Daud, A.A. Aziz, Appl. Catal. A Gen. 470 (2014) 140–161, https://doi.org/10.1016/j.apcata.2013.10.052.
[6] F. Su, Y. Guo, Green Chem. 16 (2014) 2934–2957, https://doi.org/10.1039/C3GC42333F.
[7] S. Rostamnia, E. Doustkhah, J. Mol. Catal. A Chem. 411 (2016) 317–324, https://doi.org/10.1016/j.molcata.2015.11.002.
[8] P. Gupta, S. Paul, Catal. Today 236 (2014) 153–170, https://doi.org/10.1016/j.cattod.2014.04.010.
[9] (a) J.K. Bashkin, Curr. Opin. Chem. Biol. 3 (1999) 752–758, https://doi.org/10.1016/S1367-5931(99)00036-8;
(b) T.P. Begley, Acc. Chem. Res. 27 (1994) 394–401, https://doi.org/10.1021/ar00048a002;

(c) B. Atashkar, M. A.Zolfigol, S. Mallakpour, Mol. Catal. 452 (2018) 192–246, https://doi.org/10.1016/j.mcat.2018.03.009.
[10] M. Zarei, H. Sepehrmansourie, M.A. Zolfigol, R. Karamian, S.H.M. Farida, New J. Chem. 42 (2018) 14308–14317, https://doi.org/10.1039/C8NJ02470G.
[11] S. Moradi, M.A. Zolfigol, M. Zarei, D.A. Alonso, A. Khoshnood, ChemistrySelect 3 (2018) 3042–3047, https://doi.org/10.1002/slct.201702544.
[12] (a) M. Li, F. Wu, Y. Gu, Chin. J. Catal 40 (2019) 1135–1140, https://doi.org/10.1016/S1872-2067(19)63370-X;
(b) S. Chen, R. Bai, M. Li, P. Liu, Y. Gu, Chem. Rec. (2020), https://doi.org/10.1002/tcr.202000097;
(c) E. Doustkhah, J. Lin, S. Rostamnia, C. Len, R. Luque, X. Luo, Y. Bando, K.C. W. Wu, J. Kim, Y. Yamauchi, Chem. Eur. J. 25 (2019) 1614–1635, https://doi.org/10.1002/chem.201802183;
(d) S. Rostamnia, E. Doustkhah, Nanochem. Res 1 (2016) 19–32, https://doi.org/10.7508/ncr.2016.01.003.
[13] F. Vetica, R.M. de Figueiredo, M. Orsini, D. Tofani, T. Gasperi, Synthesis 47 (2015) 2139–2184, https://doi.org/10.1055/s-0034-1378742.
[14] (a) W. Waring, A. Convery, V. Mishra, A. Shenkin, D. Webb, S. Maxwell, Clin. Sci. 105 (2003) 425–430, https://doi.org/10.1042/CS20030149;
(b) S. Verma, J. Choudhary, K.P. Singh, P. Chandra, S.P. Singh, Int. J. Biol. Macromol. 130 (2019) 333–341, https://doi.org/10.1016/j.ijbiomac.2019.02.121;
(c) T.A. Silva, M.R.K. Khan, O. Fatibello-Filho, M.M. Collinson, J. Electroanal. Chem. 846 (2019) 113160, https://doi.org/10.1016/j.jelechem.2019.05.042.
[15] (a) H. Liu, G.P. Reynolds, X. Wei, J. Alzheimer's Dis (2020) 1–7, https://doi.org/10.3233/JAD-191111;
(b) S.I. Kaya, S. Kurbanoglu, S.A. Ozkan, Crit. Rev. Anal. Chem. 49 (2019) 101–125, https://doi.org/10.1080/10408347.2018.1489217;
(c) K. Davies, A. Sevanian, S. Muakkassah-Kelly, P. Biochem. J. 235 (1986) 747–754, https://doi.org/10.1042/bj2350747;
(d) Z. Cai, Y. Ye, X. Wan, J. Liu, S. Yang, Y. Xia, G. Li, Q. He, Nanomaterials 9 (2019) 835, https://doi.org/10.3390/nano9060835;
(e) C.J. Bailey, Diabetes Obes. Metab. 21 (2019) 1291–1298, https://doi.org/10.1111/dom.13670;
(f) H. Karimi-Maleh, O.A. Arotiba, J. Colloid Interface Sci. 560 (2020) 208–212, https://doi.org/10.1016/j.jcis.2019.10.007.
[16] J.B. Marcus, Vitamin and mineral basics: the ABCs of healthy foods and beverages, including phytonutrients and functional foods: healthy vitamin and mineral choices, roles and applications in nutrition, food science and the culinary arts. ch. 7, food science and the culinary arts, in: J.B. Marcus (Ed.), Culinary Nutrition: the Science and Practice of Healthy Cooking, Academic Press, Boca Raton, 2013, pp. 279–331.
[17] A. Badora, K. Bawolska, J. Kozłowska-Strawska, J. Domańska, Food Additives in Food Products: A Case Study, Nutrition in Health and Disease-Our Challenges Now and Forthcoming Time, IntechOpen, 2019, https://doi.org/10.5772/intechopen.85723.
[18] Y. Liu, J. Chen, Phosphorus cycle, in: B. Fath (Ed.), Encyclopedia of Ecology, second edition, Elsevier, Oxford, 2014, pp. 181–191.
[19] (a) H. Sepehrmansouri, M. Zarei, M.A. Zolfigol, A.R. Moosavi-Zare, S. Rostamnia, S. Moradi, Mol. Catal. 481 (2020) 110303, https://doi.org/10.1016/j.mcat.2019.01.023;
(b) S. Babaee, M. Zarei, M.A. Zolfigol, S. Khazalpour, M. Hasani, U. Rinner, R. Schirhagl, N. Norouzi, S. Rostamnia, RSC Adv. 11 (2021) 2141, https://doi.org/10.1039/d0ra06674e;
(c) H. Sepehrmansourie, M. Zarei, M.A. Zolfigol, S. Babaee, S. Rostamnia, Sci. Rep. 11 (2021) 5279, https://doi.org/10.1038/s41598-021-84005-2.
[20] S.M. Sanad, A.A. Ahmed, A.E. Mekky, J. Heterocycl. Chem. 57 (2020) 590–605, https://doi.org/10.1002/jhet.3789.
[21] D. Baek, H. Ryu, J.Y. Ryu, J. Lee, B.M. Stoltz, S. Hong, Chem. Sci. 11 (2020) 4602–4607, https://doi.org/10.1039/D0SC00412J.
[22] M.A. Radwan, M.A. Alshubramy, M. Abdel-Motaal, B.A. Hemdan, D.S. El-Kady, Bioorg. Chem. 96 (2020) 103516, https://doi.org/10.1016/j.bioorg.2019.103516.
[23] A.E. Mekky, S.M. Sanad, Synth. Commun. 49 (2019) 1385–1395, https://doi.org/10.1080/00397911.2019.1595658.
[24] Y.-C. Zhang, F. Jiang, F. Shi, Acc. Chem. Res. 53 (2019) 425–446, https://doi.org/10.1021/acs.accounts.9b00549.
[25] N. Kaur, Synth. Commun. 45 (2015) 1145–1182, https://doi.org/10.1080/00397911.2013.827208.
[26] T. Ding, F. Tang, G. Ni, J. Liu, H. Zhao, Q. Chen, RSC Adv. 10 (2020) 6223–6248, https://doi.org/10.1039/C9RA09427J.
[27] Y. Zong, H. Shao, Y. Pang, D. Wang, K. Liu, L. Wang, J. Mol. Struct. 1115 (2016) 187–198, https://doi.org/10.1016/j.molstruc.2016.02.095.
[28] P. Panahi, N. Nouruzi, E. Doustkhah, H. Mohtasham, A. Ahadi, A. Ghiasi-Moaser, S. Rostamnia, G. Mahmoudi, A. Khataee, Ultrason. Sonochem. 58 (2019) 104653, https://doi.org/10.1016/j.ultsonch.2019.104653.
[29] R. Gujjarappa, N. Vodnala, C. Malakar, ChemistrySelect 5 (2020) 8745–8758, https://doi.org/10.1002/slct.202002765.
[30] H. Nishiyama, Y. Itoh, H. Matsumoto, S.-B. Park, K. Itoh, J. Am. Chem. Soc. 116 (1994) 2223–2224, https://doi.org/10.1021/ja00084a104.
[31] S.V. Bhaskaruni, S. Maddila, K.K. Gangu, S.B. Jonnalagadda, Arab. J. Chem. 13 (2020) 1142–1178, https://doi.org/10.1016/j.arabjc.2017.09.016.
[32] Y. Kaddouri, F. Abrigach, E.B. Yousfi, M. El Kodadi, R. Touzani, Heliyon 6 (2020) e03185, https://doi.org/10.1016/j.heliyon.2020.e03185.
[33] S.A. Sharma, P. Sudhindra, N. Roy, P. Paira, InorganicaChim. Acta (2020) 119925, https://doi.org/10.1016/j.ica.2020.119925.
[34] S. Ando, N. Nakano, H. Matsunaga, T. Ishizuka, J. Organomet. Chem. (2020), 121200, https://doi.org/10.1016/j.jorganchem.2020.121200.
[35] C. Allais, J.-M. Grassot, J. Rodriguez, T. Constantieux, Chem. Rev. 114 (2014) 10829–10868, https://doi.org/10.1021/cr500099b.
[36] (a) S.-Y. Wang, X.-C. Shi, P. Laborda, Eur. J. Med. Chem. 185 (2020) 111847, https://doi.org/10.1016/j.ejmech.2019.111847;
(b) W. Xie, E. Pakdel, Y. Liang, Y.J. Kim, D. Liu, L. Sun, X. Wang, Biomacromolecules 20 (2019) 4312–4331, https://doi.org/10.1021/acs.biomac.9b01413;
(c) H.M. Lee, P.L. Chiu, C.-H. Hu, C.-L. Lai, Y.-C. Chou, J. Organomet. Chem. 690 (2005) 403–414, https://doi.org/10.1016/j.jorganchem.2004.09.053;
(d) A.A. Fadda, A. El-Mekabaty, I.A. Mousa, K.M. Elattar, Synth. Commun. 44 (2014) 1579–1599, https://doi.org/10.1080/00397911.2013.861915.
[37] M. Shiri, Chem. Rev. 112 (2012) 3508–3549, https://doi.org/10.1021/cr2003954.
[38] M. Shiri, M.A. Zolfigol, H.G. Kruger, Z. Tanbakouchian, Chem. Rev. 110 (2010) 2250–2293, https://doi.org/10.1021/cr900195a.
[39] I.V. Alabugin, Stereoelectronic Effects, A Bridge Between Structure and Reactivity, 2016, https://doi.org/10.1002/9781118906378. Chapter 4.
[40] T. Harris, D.M. Chenoweth, J. Am. Chem. Soc. 141 (2019) 18021–18029, https://doi.org/10.1021/jacs.9b05524.
[41] K.B. Wiberg, W.F. Bailey, K.M. Lambert, Z.D. Stempel, The anomeric effect: it's complicated, J. Org. Chem. 83 (2018) 5242–5255, https://doi.org/10.1021/acs.joc.8b00707.
[42] E. Juaristi, R. J. Org. Chem. 83 (2018) 10326–10333, https://doi.org/10.1021/acs.joc.8b01458.
[43] E. Juaristi, R. Notario, J. Org. Chem. 83 (2018) 3293–3298, https://doi.org/10.1021/acs.joc.8b00220.
[44] E. Juaristi, R. Notario, J. Org. Chem. 81 (2016) 1192–1197, https://doi.org/10.1021/acs.joc.5b02718.
[45] A.R. Katritzky, P.J. Steel, S.N. Denisenko, Tetrahedron 57 (2001) 3309–3314, https://doi.org/10.1016/S0040-4020(01)00218-6.
[46] F. Karimi, M. Yarie, M.A. Zolfigol, Mol. Catal. 489 (2020) 110924, https://doi.org/10.1016/j.mcat.2020.110924.
[47] J. Afsar, M.A. Zolfigol, A. Khazaei, M. Zarei, Y. Gu, D.A. Alonso, A. Khoshnood, Mol. Catal. 482 (2020) 110666, https://doi.org/10.1016/j.mcat.2019.110666.
[48] S. Babaee, M. Zarei, H. Sepehrmansourie, M.A. Zolfigol, S. Rostamnia, ACS Omega 5 (2020) 6240–6249, https://doi.org/10.1021/acsomega.9b02133.
[49] F. Jalili, M. Zarei, M.A. Zolfigol, S. Rostamnia, A.R. Moosavi-Zare, Microporous Mesoporous Mater. 294 (2020) 109865, https://doi.org/10.1016/j.micromeso.2019.109865.
[50] P. Ghasemi, M. Yarie, M.A. Zolfigol, A.A. Taherpour, M. Torabi, ACS Omega 5 (2020) 3207–3217, https://doi.org/10.1021/acsomega.9b03277.
[51] F. Karimi, M. Yarie, M.A. Zolfigol, RSC Adv. 10 (2020) 25828–25835, https://doi.org/10.1039/D0RA04461J.
[52] M. Dashteh, M.A. Zolfigol, A. Khazaei, S. Baghery, M. Yarie, S. Makhdoomi, M. Safaiee, RSC Adv. 10 (2020) 27824–27834, https://doi.org/10.1039/D0RA02172E.
[53] (a) M. Yarie, Iran. J. Catal. 7 (2017) 85–88;
(b) M. Yarie, Iran. J. Catal. 10 (2020) 79–83.
[54] M.A. Zolfigol, A. Khazaei, S. Alaie, S. Baghery, F. Maleki, Y. Bayat, A. Asgari, RSC Adv. 6 (2016) 58667–58679, https://doi.org/10.1039/C6RA13231F.
[55] M.A. Zolfigol, F. Afsharnadery, S. Baghery, S. Salehzadeh, F. Maleki, RSC Adv. 5 (2015) 75555–75568, https://doi.org/10.1039/C5RA16289K.
[56] Y.-Y. Sheng, J. Xiang, Z.-S. Wang, J. Jin, Y.-Q. Wang, Q.-S. Li, D. Li, Z.-T. Fang, J.-L. Lu, J.-H. Ye, Y.-R. Liang, X.-Q. Zheng, Front. Nutr. 7 (2020) 596823, https://doi.org/10.3389/fnut.2020.596823.
[57] J. Slaett, I. Romero, J. Bergman, Cyanoacetylation of indoles, pyrroles and aromatic amines with the combination cyanoacetic acid and acetic anhydride, Synthesis (Stuttgart) (2004) 2760–2765.
[58] P. Laoharojanaphand, T. Lin, J.O. Stoffer, J. Appl. Polym. Sci. 40 (1990) 369–384, https://doi.org/10.1002/app.1990.070400306.
[59] P. Shih, S. Yung, T. Chin, J. Non Cryst. Solids 244 (1999) 211–222, https://doi.org/10.1016/S0022-3093(99)00011-3.
[60] K. Mequanint, R. Sanderson, H. Pasch, J. Appl. Polym. Sci. 88 (2003) 900–907, https://doi.org/10.1002/app.11680.
[61] S. Babaee, M.A. Zolfigol, M. Zarei, J. Zamanian, ChemistrySelect 3 (2018) 8947–8954, https://doi.org/10.1002/slct.201801476.
[62] A.R. Moosavi-Zare, M.A. Zolfigol, M. Zarei, A. Zare, V. Khakyzadeh, A. Hasaninejad, Appl. Catal. A Gen. 467 (2013) 61–68, https://doi.org/10.1016/j.apcata.2013.07.004.
[63] H. Sepehrmansourie, M. Zarei, R. Taghavi, M.A. Zolfigol, ACS Omega 4 (2019) 17379–17392, https://doi.org/10.1021/acsomega.9b02135.
[64] M. Zarei, M.A. Zolfigol, A.R. Moosavi-Zare, E. Noroozizadeh, J. Iran. Chem. Soc. 14 (2017) 2187–2198, https://doi.org/10.1007/s13738-017-1155-4.
[65] M. Rajabi-Salek, M.A. Zolfigol, M. Zarei, Res. Chem. Intermed. 44 (2018) 5255–5269, https://doi.org/10.1007/s11164-018-3421-1.
[66] (a) M.A. Zolfigol, Tetrahedron 57 (2001) 9509–9511, https://doi.org/10.1016/S0040-4020(01)00960-7;
(b) H. Sepehrmansourie, Iran. J. Catal. 10 (2020) 175–179.
[67] E. Noroozizadeh, A.R. Moosavi-Zare, M.A. Zolfigol, M. Zarei, R. Karamian, M. Asadbegy, S. Yari, S.H.M. Farida, J. Iran. Chem. Soc. 15 (2018) 471–481, https://doi.org/10.1007/s13738-017-1247-1.